MODES OF VIBRATION

OF

PIEZOELECTRIC QUARTZ CRYSTALS

by

ARTHUR L. BENNETT

Project B - 214

Engineering Experiment Station
Georgia Institute of Technology
Atlanta, 1961 - 63

CONTENTS

FINAL REPORT

PROJECT B-214

MODES OF VIBRATION OF PIEZOELECTRIC QUARTZ CRYSTALS

ARTHUR L. BENNETT

Research Grant NSF-G18972

1 July 1961 to 30 September 1963

Prepared for
National Science Foundation
Washington, D. C.

1963

Engineering Experiment Station
GEORGIA INSTITUTE OF TECHNOLOGY
Atlanta, Georgia

ENGINEERING EXPERIMENT STATION
GEORGIA INSTITUTE OF TECHNOLOGY
Atlanta 13, Georgia

INTERIM TECHNICAL REPORT NO. 1

PROJECT NO. B-214

COUPLED THICKNESS-SHEAR AND FLEXURE VIBRATIONS IN RECTANGULAR AT-CUT QUARTZ PLATES

By

Gilbert C. Knollman*

1 March 1962

NATIONAL SCIENCE FOUNDATION
Washington, D. C.
RESEARCH GRANT NSF-G18972

*Dr. Knollman is now with Lockheed Missiles and Space Co.,
Palo Alto, California

ABSTRACT

This report provides background information and details in the development of an analytical study of coupled thickness-shear and flexure vibration modes of rectangular, AT-cut quartz plates. The theoretical approach involves a variational technique which allows for considerable refinement of the mathematical analysis over that heretofore published in the literature. General stress-strain and piezoelectric relations are first introduced and then simplified to the forms appropriate for quartz. A convenient rectangular coordinate system is chosen and the Lagrangian formulation presented. At this point, the procedure taken by Mindlin, together with his basic assumptions, is outlined for comparison. Next, several intuitive assumptions and mathematical models are considered. Various assumptions and models are combined for analysis, and each combination is studied to determine its plausibility as a representation of the resonance phenomenon of interest. Mathematical details are included for the model ultimately selected as most descriptive of the vibration modes under discussion, and the calculated resonance chart is found to display excellent agreement with the recent experimental results of Koga. For convenience, all numerical constants involved in the theory are tabulated in an appendix.

CONTENTS

List of Figures

COUPLED THICKNESS-SHEAR AND FLEXURE VIBRATIONS IN RECTANGULAR AT-CUT QUARTZ PLATES

1. Introduction

The piezoelectric effect can be defined as an electric polarization produced by mechanical strain in crystals belonging to certain classes, the polarization being proportional to the strain and changing sign with it. This statement in actuality defines the so-called "direct piezoelectric effect." Closely related to it is the "converse effect" (sometimes called the "reciprocal" or "inverse" effect), whereby a piezoelectric crystal, when electrically polarized, becomes strained in an amount proportional to the polarizing field. Both effects are manifestations of the same fundamental property of the crystal, and they occupy a position among those physical phenomena which are reversible.

Among the many practical applications of piezoelectric crystals may be mentioned their almost universal use in radio transmitting stations, either for direct control of frequency in the form of piezo oscillators or indirectly as monitoring devices. The combination in quartz of extraordinarily low damping with sufficiently strong piezoelectric properties to react upon and control the frequency of vacuum-tube generators results in a method for obtaining frequencies which are much more constant than those obtained by electrical tuning alone. Frequency variation with temperature can be largely avoided by cutting quartz plates according to special orientations. Low temperature-coefficient quartz crystals known as AT and BT cuts need no temperature control for most uses, or only a very simple one for the most exacting conditions. AT and BT plates, operated as thickness-shear resonators, are employed in the control of radio-frequency oscillators in the range from 1 to 10 megacycles, the AT plate being most useful in the lower part of the range. Filters on pilot channels for the coaxial telephone system often involve the AT-cut plate.

The frequency to excite a given crystal in a thickness-shear mode of vibration can correspond to a harmonic or overtone frequency of one or more types of motion different in character from the thickness-shear class. Coupling is then said to exist between the thickness-shear mode and these other modes of motion. In the case of an AT-cut crystal, thickness-shear modes may be rather strongly coupled to flexure modes of motion, and the crystal must be exactly dimensioned in order to minimize such interactions.

In the discussion which follows, attention is focused on a rectangular AT-cut quartz plate. Of primary interest are the high-frequency shear vibrations (in the vicinity of the fundamental thickness-shear mode) and the flexure modes (along the crystal's length) which are coupled to them. Figure 1 contains several diagrams illustrating isolated flexure modes of motion along the length of a rectangular plate as well as the fundamental thickness-shear mode and its first two inharmonics.* As evidenced later, the high even orders of flexure are strongly coupled to the fundamental thickness-shear mode and its odd inharmonics.

An early investigation [1]** revealed that the fundamental thickness-shear frequency can be approximated analytically by considering the plate to be infinitely large compared with its thickness. Later reports [2,3] included mode computations for AT-cut quartz plates of finite length-to-thickness ratio which displayed, both qualitatively and quantitatively, the intricate high-frequency spectrum observed in the laboratory. Finite-plate theory was further extended by Mindlin [4] to accomodate the piezoelectric effect by including the interaction between elastic and electric fields in the vibrating crystal. All of this early work, however, was based on the direct mathematical approach of solving appropriate differential equations of motion. The present report expounds the variational technique more recently adopted by Koga [5], which allows for considerable refinement in the mathematical analysis. The theoretical results obtained by this method are found to agree much better with experiment than do those given in the aforementioned papers.

For purposes of comparison, the direct differential-equation approach as exploited by Mindlin will be briefly outlined herein and note made of its basic assumptions and limitations. Also reviewed are several alternative sets of assumptions and associated mathematical models which were analyzed in the course of arriving at an "optimum" variational solution. This final model is considered in detail, and a plot is given of resonance modes computed therefrom, as compared with recent experimental data.

---

*The term "inharmonic" is used herein to designate the order of subdivision of the fundamental thickness-shear motion within the length dimension, as indicated in Figure 1b.

**A number in brackets in the text refers to an entry in the Bibliography found at the end of this report.

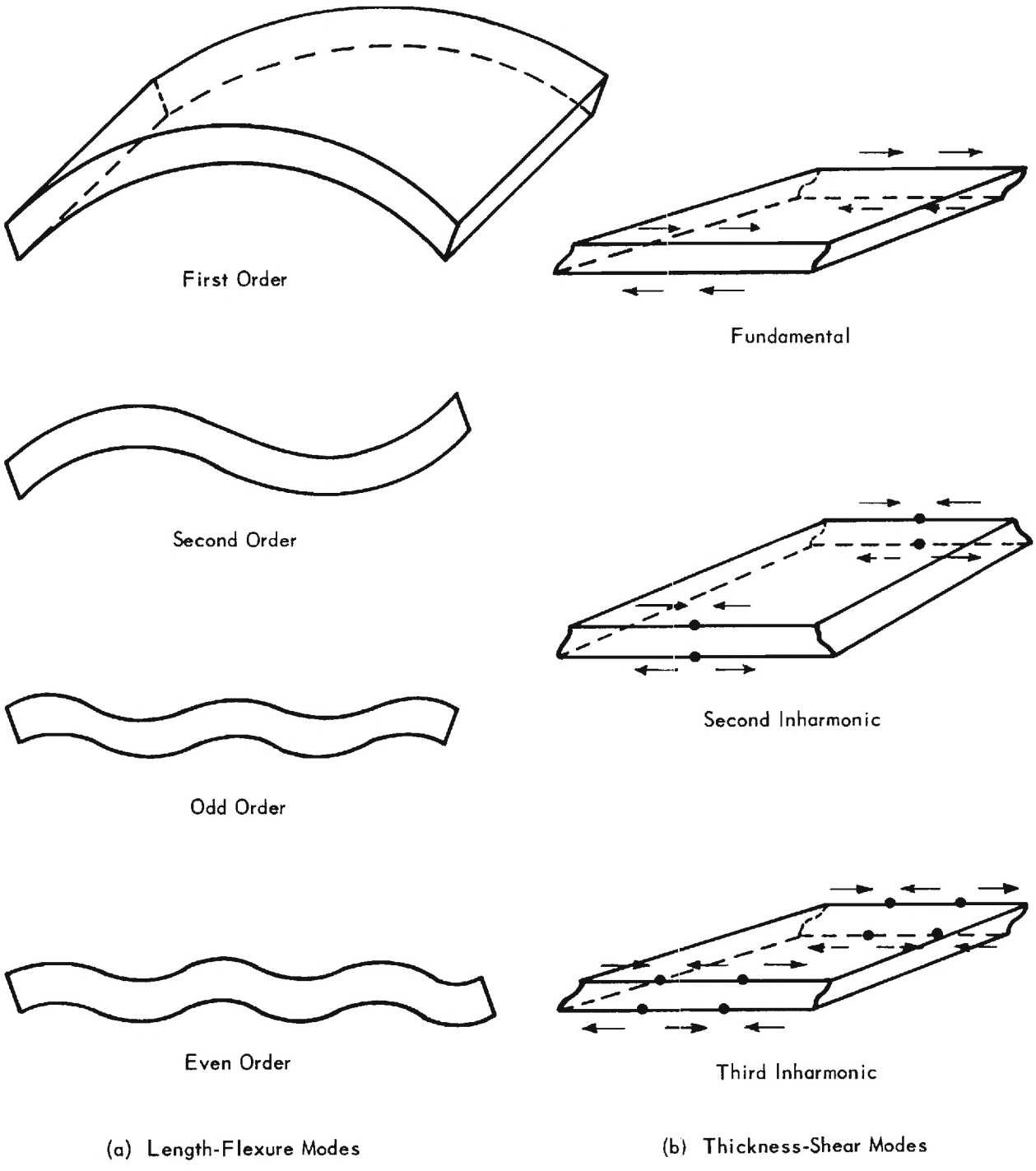

Figure 1. Deformation of a Rectangular Plate in Flexure and in High-Frequency Shear.

2. Problem Geometry

Figure 2a displays, in accordance with the 1945 IRE standard, the three crystallographic axes X, Y, Z of a quartz crystal. The optic or Z-axis is parallel to the long direction of the crystal and is the so-called principal axis; the X-axis lies through one of the apexes of the hexagonal face and is the electrical or digonal axis; the Y-axis is normal to the other two in a right-handed coordinate system.

For an AT-cut quartz plate, the thickness direction is inclined to the optic axis at an angle θ as shown in Figure 2b. This inclination angle, determined experimentally, lies between 54°41' and 54°45' and is chosen to yield a crystal resonator with zero temperature-coefficient of frequency. To a close approximation, the angle θ is given by

$$\theta = \text{Cos}^{-1} \frac{1}{\sqrt{3}} . \qquad (1)$$

The right-handed Cartesian coordinate system x,y,z of Figure 2c is that upon which the subsequent mathematical development is formulated. In this system, with origin at the geometrical center of the rectangular plate to be analyzed, the y-axis is in the thickness direction of the plate, while the x-axis is parallel to the crystallographic X-axis. The dimensions of the rectangular plate are as depicted. Insofar as the elastic, piezoelectric, and dielectric constants of the crystal plate are concerned, the x,y,z frame constitutes a coordinate system which is rotated counterclockwise about the crystallographic X-axis by an angle $(\frac{\pi}{2} - \theta)$.

3. Fundamental Elastic and Piezoelectric Equations

For small displacements within an elastic, piezoelectric solid body, the components of stress at any point of the body are related to the strains at that point by equations of the form [6a, 7a]

$$T_a^o = c_{ab} e_b + \bar{T}_a \quad , \qquad (a,b = 1 \text{ to } 6) \qquad (2)^*$$

where superscript "o" signifies a combination of mechanical and piezoelectric quantities. In Equation (2), a generalized Hooke's Law, c_{ab} is an elastic coeffi-

*Unless otherwise noted, the Einstein convention is employed throughout--that is, a repeated index in a term indicates for this term a summation with respect to the index.

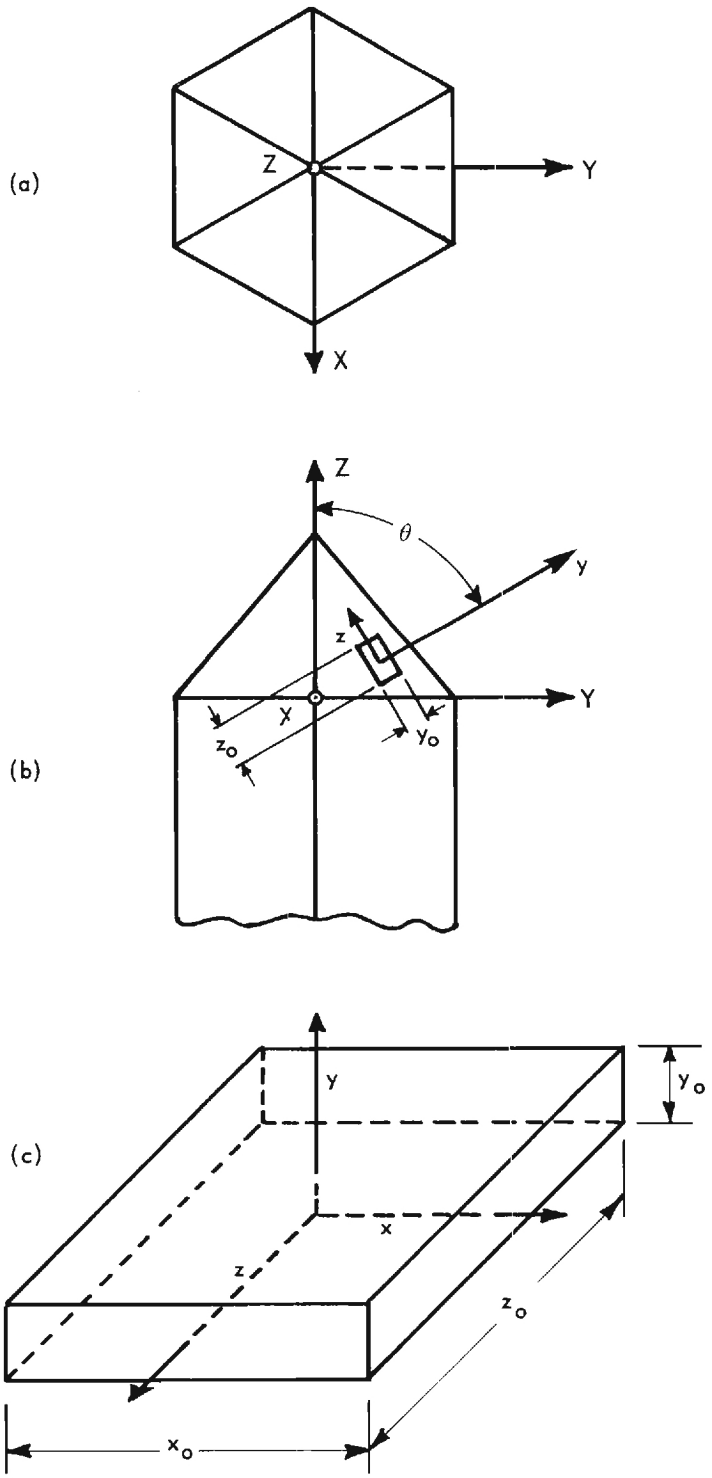

Figure 2. (a) Crystallographic Axes of Quartz;
(b) Orientation of a Rectangular, AT-Cut Quartz Plate;
(c) Problem Coordinate System.

cient expressing proportionality between the strain e_b and the mechanical stress in the absence of any other strains. Since the internal energy is a perfect differential, it follows that $c_{ab} = c_{ba}$ [6b]. The overscored quantity on the right of Equation (2) is an equivalent mechanical stress arising from the piezoelectric effect and is given by [7a]

$$\bar{T}_a = \varepsilon_{da} E_d \quad , \qquad (d = 1 \text{ to } 3) \tag{3}$$

where E_d is a component of the effective electric field existing in the crystal and ε_{da} denotes a piezoelectric stress coefficient. It is noted that, in general, $\varepsilon_{da} \neq \varepsilon_{ad}$ [7b].

The effective electric field is attributed to the polarization of the piezoelectric crystalline medium. By introducing coefficients of dielectric stiffness γ_{dk}, one can express the components E_d of field strength in the crystal in terms of polarization components P_k [7c]:

$$E_d = \gamma_{dk} P_k \quad . \qquad (k = 1 \text{ to } 3) \tag{4}$$

Here $\gamma_{dk} = \gamma_{kd}$. Polarization, in turn, is related to strain by the relation [7d]

$$P_k = \varepsilon_{k\ell} e_\ell \quad , \qquad (\ell = 1 \text{ to } 6) \tag{5}$$

which expresses the electric moment per unit volume induced by a mechanical strain.

4. Relations for Rectangular, AT-Cut Quartz Crystals

The elastic and piezoelectric relationships contained in the previous section can be applied to any orthogonal coordinate system. When referred to the coordinate system of Figure 2c, the strains e_b are defined in terms of the displacements $u(x,y,z,t)$, $v(x,y,z,t)$, $w(x,y,z,t)$ along the respective axes x,y,z as follows:

$$\begin{aligned} e_1 &= \frac{\partial u}{\partial x} , \qquad e_2 = \frac{\partial v}{\partial y} , \qquad e_3 = \frac{\partial w}{\partial z} , \\ e_4 &= \frac{\partial w}{\partial y} + \frac{\partial v}{\partial z} , \qquad e_5 = \frac{\partial w}{\partial x} + \frac{\partial u}{\partial z} , \qquad e_6 = \frac{\partial v}{\partial x} + \frac{\partial u}{\partial y} . \end{aligned} \tag{6}$$

The first three of the e_b are tension strains, or elongations per unit length, while the latter three designate total shearing strains about the three coordinate axes.

Certain of the elastic, piezoelectric, and dielectric constants introduced previously vanish for a crystal with trigonal symmetry (such as quartz) and where the x-axis is a binary axis of symmetry. Thus, in view of the coordinate system in Figure 2c [7e,8,9a,9b],

$$\begin{gathered} c_{15} = c_{16} = c_{25} = c_{26} = c_{35} = c_{36} = c_{45} = c_{46} = 0 \ , \\ \varepsilon_{15} = \varepsilon_{16} = \varepsilon_{21} = \varepsilon_{22} = \varepsilon_{23} = \varepsilon_{24} = \varepsilon_{31} = \varepsilon_{32} = \varepsilon_{33} = \varepsilon_{34} = 0 \ , \\ \gamma_{12} = \gamma_{13} = 0 \ . \end{gathered} \tag{7}$$

Equations (2) can now be expanded to read

$$\begin{aligned} T_1^o &= c_{11}e_1 + c_{12}e_2 + c_{13}e_3 + c_{14}e_4 + \bar{T}_1 \ , \\ T_2^o &= c_{21}e_1 + c_{22}e_2 + c_{23}e_3 + c_{24}e_4 + \bar{T}_2 \ , \\ T_3^o &= c_{31}e_1 + c_{32}e_2 + c_{33}e_3 + c_{34}e_4 + \bar{T}_3 \ , \\ T_4^o &= c_{41}e_1 + c_{42}e_2 + c_{43}e_3 + c_{44}e_4 + \bar{T}_4 \ , \\ T_5^o &= c_{55}e_5 + c_{56}e_6 + \bar{T}_5 \ , \\ T_6^o &= c_{65}e_5 + c_{66}e_6 + \bar{T}_6 \ , \end{aligned} \tag{8}$$

where, from (3),

$$\begin{gathered} \bar{T}_1 = \varepsilon_{11}E_1 \ , \quad \bar{T}_2 = \varepsilon_{12}E_1 , \quad \bar{T}_3 = \varepsilon_{13}E_1 , \quad \bar{T}_4 = \varepsilon_{14}E_1 \ , \\ \bar{T}_5 = \varepsilon_{25}E_2 + \varepsilon_{35}E_3 , \quad \bar{T}_6 = \varepsilon_{26}E_2 + \varepsilon_{36}E_3 \ . \end{gathered} \tag{9}$$

Similarly, Equations (4) and (5) become

$$E_1 = \gamma_{11}P_1 \ , \quad E_2 = \gamma_{22}P_2 + \gamma_{23}P_3 \ , \quad E_3 = \gamma_{23}P_2 + \gamma_{33}P_3 \ ; \tag{10}$$

$$P_1 = \varepsilon_{11}e_1 + \varepsilon_{12}e_2 + \varepsilon_{13}e_3 + \varepsilon_{14}e_4 \ ,$$

$$P_2 = \varepsilon_{25}e_5 + \varepsilon_{26}e_6 \ , \qquad (11)$$

$$P_3 = \varepsilon_{35}e_5 + \varepsilon_{36}e_6 \ .$$

In the above, T_m^o, e_m, E_m, and P_m are components of stress, strain, electric force and polarization, respectively, along the axes x,y,z of Figure 2c. These components are sometimes written in the equivalent notation given below:

$$T_1^o = X_x^o \ , \quad e_1 = e_{xx} \ , \quad E_1 = E_x \ ,$$

$$T_2^o = Y_y^o \ , \quad e_2 = e_{yy} \ , \quad E_2 = E_y \ ,$$

$$T_3^o = Z_z^o \ , \quad e_3 = e_{zz} \ , \quad E_3 = E_z \ ,$$

$$T_4^o = Y_z^o \ , \quad e_4 = e_{yz} \ , \quad P_1 = P_x \ ,$$

$$T_5^o = X_z^o \ , \quad e_5 = e_{xz} \ , \quad P_2 = P_y \ ,$$

$$T_6^o = X_y^o \ , \quad e_6 = e_{xy} \ , \quad P_3 = P_z \ .$$

Results cited in Equations (8) and (9) agree with those of Mindlin [4], while those in (10) and (11) differ. Mindlin expresses the electric field as the negative gradient of the electrostatic potential, and then relates potential and polarization through Poisson's equation. Furthermore, he includes, in the expressions for polarization components in terms of strains, relations involving as products the dielectric susceptibility and electric field components. It is argued by the present writer that the mechanical strain produces a piezoelectrically-induced polarization which, in turn, can be considered as an effective electric field existing through the dielectric. Hence, the form of Equations (10) and (11) above.

5. Variational Equation of Motion

According to Hamilton's Principle for a conservative system, the motion of the system from time t_1 to time t_2 is such that the line integral of the

Lagrangian is an extremum. Expressed mathematically,

$$\delta \int_{t_1}^{t_2} L \, dt = 0 \tag{12}$$

where L is the familiar Lagrangian, expressible in terms of the total kinetic energy T and the potential energy V of the system--namely,

$$L = T - V \quad . \tag{13}$$

With reference to the coordinate system in Figure 2c, we write for the kinetic energy in the case of small displacements, to which our entire discussion is limited,

$$T = \iiint \frac{\rho}{2}\left[\left(\frac{\partial u}{\partial t}\right)^2 + \left(\frac{\partial v}{\partial t}\right)^2 + \left(\frac{\partial w}{\partial t}\right)^2\right] dx \, dy \, dz \quad , \tag{14}$$

where, as previously noted, u,v,w are displacements along the axes x,y,z, respectively; ρ denotes the density in the unstrained state. The variation of the kinetic energy term in (12) can be performed to obtain [10a]

$$\delta \int_{t_1}^{t_2} T \, dt = \int_{t_1}^{t_2} dt \iiint \rho\left(\frac{\partial u}{\partial t}\frac{\partial}{\partial t}\delta u + \frac{\partial v}{\partial t}\frac{\partial}{\partial t}\delta v + \frac{\partial w}{\partial t}\frac{\partial}{\partial t}\delta w\right) dx \, dy \, dz \quad . \tag{15}$$

Integration by parts is next introduced. For example,

$$\int_{t_1}^{t_2} \frac{\partial u}{\partial t}\frac{\partial}{\partial t}\delta u \, dt = \left[\frac{\partial u}{\partial t}\delta u\right]_{t_1}^{t_2} - \int_{t_1}^{t_2} \frac{\partial^2 u}{\partial t^2}\delta u \, dt \quad , \tag{16a}$$

$$= -\int_{t_1}^{t_2} \frac{\partial^2 u}{\partial t^2}\delta u \, dt \tag{16b}$$

since the infinitesimal variation δu of u vanishes for both the initial and final values of t (from the restrictions apropos to the variational problem).

Similarly, δv and δw vanish at t_1 and t_2. Equation (15) now reads

$$\delta \int_{t_1}^{t_2} T \, dt = - \int_{t_1}^{t_2} dt \iiint \rho \left(\frac{\partial^2 u}{\partial t^2} \delta u + \frac{\partial^2 v}{\partial t^2} \delta v + \frac{\partial^2 w}{\partial t^2} \delta w \right) \, dx \, dy \, dz. \tag{17}$$

Here one introduces the function W, which represents the potential energy per unit volume stored in the crystal when in a strained state. The potential energy V in Equation (13) is then written [10a]

$$V = \iiint W \, dx \, dy \, dz. \tag{18}$$

Love [10b] describes the quantity W as a "strain-energy-function." If changes of state take place adiabatically--that is to say, in such a way that no heat is gained or lost by any element of the body--the function W has the property

$$T_a^o = \frac{\partial W}{\partial e_a}, \tag{19}$$

and an expression for 2W can be written in the form [10c]

$$2W = T_a^o e_a \tag{20}$$

Taking the variation of the potential energy given by (18), we have

$$\delta V = \iiint \delta w \, dx \, dy \, dz.$$

Introducing this result together with the right member of (17) into Equation (12), we subsequently obtain the following variational equation of motion [10d]:

$$\iiint \left[\rho \left(\frac{\partial^2 u}{\partial t^2} \delta u + \frac{\partial^2 v}{\partial t^2} \delta v + \frac{\partial^2 w}{\partial t^2} \delta w \right) + \delta W \right] dx \, dy \, dz = 0 \quad . \tag{21}$$

It is noted at this point that

$$\delta W = \frac{\partial W}{\partial e_a} \delta e_a \quad , \tag{22}$$

which enables one to integrate by parts the latter expression in Equation (21). Should this be carried out, one then obtains the differential equations of motion for the system (the Euler equations of the variational problem) as well as natural boundary conditions. Both Koga [2] and Mindlin [3,4] have previously dealt with the problem of coupled thickness-shear and flexure vibrations in rectangular, AT-cut quartz plates, and have utilized the differential equations as a point of departure. In the present analysis, however, Equation (21) forms the foundation upon which the subsequent mathematical development is constructed. This approach makes it unnecessary to assume that the displacements bear a simple y-dependence, as required for solution of the equations of motion.

6. The Mindlin Procedure

Before introducing the simplifying assumptions used herein, an outline is presented of the basic postulates and procedures adopted by Mindlin [4]. His theory includes the interaction between elastic and electric fields in a vibrating, rectangular, AT-cut quartz crystal, as does the present approach. However, although Equations (8) and (9) above enter into Mindlin's work, different versions of Equations (10) and (11) appear--a fact previously noted and discussed. It should be recalled also that Mindlin employs the differential equations governing the motion of the crystal, and not the variational equation derived above.

Concerning Mindlin's basic assumptions, he neglects the normal component of traction on planes parallel to the $x_o z_o$ face--i.e.,

$$T_2 = 0$$

throughout the plate. In addition, the faces are assumed to be traction-free, so that (see Figure 2c)

$$T_2 = T_4 = T_6 = 0 \quad \text{on} \quad y = \pm y_o/2 \quad .$$

A simple y-dependence is required of the displacements in order to obtain a solution of the differential equations of motion. To accommodate as well as possible the true y-dependence, which varies markedly with frequency, Mindlin introduces an arbitrary constant at an appropriate point of the development. This constant is later evaluated in the limit of an infinite plate. Since the resonant frequencies are regarded as practically independent of the z_o-dimension, the displacement w and the field E_3 are assumed to be nil and the remaining displacements are taken as z-independent. Thus,

$$u = \frac{y}{y_o} e^{i\omega t} (L_1 \sin \delta_1 x + M_1 \cos \delta_1 x + N_1 \sin \delta_2 x + Q_1 \cos \delta_2 x + R_1 x + R_2) \quad ,$$

$$v = e^{i\omega t} (L_2 \sin \delta_1 x + M_2 \cos \delta_1 x + N_2 \sin \delta_2 x + Q_2 \cos \delta_2 x) \quad ,$$

$$w = 0 \quad , \qquad E_3 = 0 \quad .$$

In the above, ω is the angular frequency of vibration while the L's, M's, N's, Q's, R's, and δ's are constants involving both the elastic and the piezoelectric constants of the crystal. In addition, Mindlin presents the electric field equations

$$E_1 = - \frac{\partial V}{\partial x} \quad , \qquad E_2 = - \frac{\partial V}{\partial y} \quad ,$$

and has for the electrostatic potential V the form

$$V = \frac{y}{y_o} e^{i\omega t} (L_3 \sin \delta_1 x + M_3 \cos \delta_1 x + N_3 \sin \delta_2 x + Q_3 \cos \delta_2 x + R_3 x + R_4) \quad .$$

Quantities L_3, M_3, N_3, Q_3, R_3, and R_4 involve the elastic and piezoelectric constants of quartz.

The above expressions constitute solutions to Mindlin's plate equations of motion derived on the basis of the assumptions noted earlier and employing Poisson's equation to relate the electrostatic potential and the polarization. Comparison of calculations made using Mindlin's theory with data obtained by Sykes [11] on resonances of rectangular AT-cut quartz plates reveals a rather consistent discrepancy. This may well be attributed to the overly simple forms chosen for the displacements.

7. A Basic Supposition

In the present approach, a fundamental supposition involves the contribution to the effective electric field of the z-component of polarization. Since P_3 is known to be uniform in the z-direction, the only charges which result from this polarization component reside on the surfaces $z = \pm z_o/2$. These charges induce, in the neighborhood of $z = \pm z_o/2$, opposite charges on the electrodes. The net result is that P_3 plays practically no role insofar as the effective electric field is concerned. (This conclusion is to be compared with the neglect of E_3 in Mindlin's theory.) Equations (10) now have the special form

$$E_1 = \gamma_{11} P_1 , \qquad E_2 = \gamma_{22} P_2 , \qquad E_3 = \gamma_{23} P_2 . \tag{23}$$

Introduction of Equation (23) into (9) then leads to

$$\bar{T}_1 = \varepsilon_{11}\gamma_{11} P_1 , \qquad \bar{T}_2 = \varepsilon_{12}\gamma_{11} P_1 , \qquad \bar{T}_3 = \varepsilon_{13}\gamma_{11} P_1 , \qquad \bar{T}_4 = \varepsilon_{14}\gamma_{11} P_1 ,$$
$$\bar{T}_5 = (\gamma_{22}\varepsilon_{25} + \gamma_{23}\varepsilon_{35}) P_2 , \qquad \bar{T}_6 = (\gamma_{22}\varepsilon_{26} + \gamma_{23}\varepsilon_{36}) P_2 . \tag{24}$$

The last two equations in (24) can be simplified through the use of transformation relations between constants pertaining to axes x,y,z of Figure 2c and the corresponding quantities as measured with respect to the crystallographic axes X, Y, Z depicted in Figure 2b. These transformations are presented in general form by Heising [12]. With primes designating quantities referred to the crystallographic axes, we obtain

$$\varepsilon_{25} = -r^2\varepsilon'_{14} + rs\varepsilon'_{11} , \qquad \varepsilon_{35} = rs\varepsilon'_{14} - s^2\varepsilon'_{11} ,$$
$$\varepsilon_{26} = -rs\varepsilon'_{14} - r^2\varepsilon'_{11} , \qquad e_{36} = s^2\varepsilon'_{14} + rs\varepsilon'_{11} ; \tag{25a}$$

$$\gamma_{11} = \gamma'_{11} , \qquad \gamma_{22} = r^2\gamma'_{11} + s^2\gamma'_{33} , \qquad \gamma_{23} = -rs(\gamma'_{11} - \gamma'_{33}) . \tag{25b}$$

In the above,

$$r = \sin\theta , \qquad s = \cos\theta , \tag{26}$$

where θ is the rotation angle displayed in Figure 2b. Substitution of (25) into the last two relations of (24) yields upon simplification

$$\bar{T}_5 = \varepsilon_{25}\gamma_{11}P_2 \ , \qquad \bar{T}_6 = \varepsilon_{26}\gamma_{11}P_2 \ . \tag{27}$$

It is noted that the dielectric stiffness coefficient normal to the principal axis is the only parameter of its class which plays a role in the present analysis.

Upon introducing Equations (11) into (27) and also into the first four relations of (24), we have

$$\begin{aligned}
\bar{T}_1 &= \varepsilon_{11}\gamma_{11}(\varepsilon_{11}e_1 + \varepsilon_{12}e_2 + \varepsilon_{13}e_3 + \varepsilon_{14}e_4) \ , \\
\bar{T}_2 &= \varepsilon_{12}\gamma_{11}(\varepsilon_{11}e_1 + \varepsilon_{12}e_2 + \varepsilon_{13}e_3 + \varepsilon_{14}e_4) \ , \\
\bar{T}_3 &= \varepsilon_{13}\gamma_{11}(\varepsilon_{11}e_1 + \varepsilon_{12}e_2 + \varepsilon_{13}e_3 + \varepsilon_{14}e_4) \ , \\
\bar{T}_4 &= \varepsilon_{14}\gamma_{11}(\varepsilon_{11}e_1 + \varepsilon_{12}e_2 + \varepsilon_{13}e_3 + \varepsilon_{14}e_4) \ , \\
\bar{T}_5 &= \varepsilon_{25}\gamma_{11}(\varepsilon_{25}e_5 + \varepsilon_{26}e_6) \ , \\
\bar{T}_6 &= \varepsilon_{26}\gamma_{11}(\varepsilon_{25}e_5 + \varepsilon_{26}e_6) \ .
\end{aligned} \tag{28}$$

Equations (8) can now be written in the form

$$T_1^o = c_{11}^o e_1 + c_{12}^o e_2 + c_{13}^o e_3 + c_{14}^o e_4 \ , \tag{29a}$$

$$T_2^o = c_{21}^o e_1 + c_{22}^o e_2 + c_{23}^o e_3 + c_{24}^o e_4 \ , \tag{29b}$$

$$T_3^o = c_{31}^o e_1 + c_{32}^o e_2 + c_{33}^o e_3 + c_{34}^o e_4 \ , \tag{29c}$$

$$T_4^o = c_{41}^o e_1 + c_{42}^o e_2 + c_{43}^o e_3 + c_{44}^o e_4 \ , \tag{29d}$$

$$T_5^o = c_{55}^o e_5 + c_{56}^o e_6 \ , \tag{29e}$$

$$T_6^o = c_{65}^o e_5 + c_{66}^o e_6 \ , \tag{29f}$$

where c^{o}_{pq} is a so-called "elasto-piezoelectric" coefficient and is defined as

$$c^{o}_{pq} = \begin{cases} c_{pq} + \gamma_{11}\varepsilon_{1p}\varepsilon_{1q} , & p,q = 1 \text{ to } 4 \\ c_{pq} + \gamma_{11}\varepsilon_{2p}\varepsilon_{2q} . & p,q = 5, 6 \end{cases} \tag{30}$$

The first term on the right side of (30) is an elastic constant while the second term is a piezoelectric stiffness parameter. It is noted that the convention adopted earlier of using superscript "o" to designate a combination of elastic and piezoelectric terms has been retained in writing Equation (30).

An experimental investigation by Koga et al [13] had as its purpose the accurate determination of elastic, piezoelectric, and dielectric stiffness constants for an AT-cut quartz plate. These constants were measured along the crystallographic axes, and numerical results are tabulated for reference in Tables B-I through B-III of Appendix B. The constants appearing in (30), however, refer to the rotated coordinate system of Figure 2c and are related to the experimental values through appropriate transformation equations [12]. Taking the rotation angle θ as that expressed in Equation (1), we have noted the corresponding transformation relations in Appendix A. These relations together with Koga's experimental values yield the elastic, piezoelectric, and dielectric stiffness constants which are recorded in Tables B-IV through B-VI. Corresponding values for the elasto-piezoelectric coefficients are obtained from Equation (30) and are listed in Table B-VII.

8. Fundamental Assumptions

Experimental studies [2] have shown that the frequencies corresponding to the particular class of coupled thickness-shear and flexure vibrations of interest here are practically independent of the crystal's z_o-dimension. Deformation is due primarily to shear and flexure in planes normal to the z-axis and almost no deformation exists in planes normal to the x-axis. Regarding x_o as considerably larger than the thickness y_o, we can arrive at two logical sets of assumptions similar in form to those of Mindlin which have been cited in Section 6. Each set is presented separately, and the group which has resulted in the best agreement between theory and experiment for coupled thickness-shear and flexure vibrations is subsequently selected as the basis for further mathematical analysis.

Set (a): $T_3^o = T_4^o = T_5^o = 0$ throughout the plate. Equation (29e) is first solved for the strain e_5, as follows:

$$e_5 = -\frac{c_{56}^o}{c_{55}^o} e_6 \ .$$

Thereupon (29f) becomes

$$T_6^o = k_1^o e_6 \ , \tag{31}$$

in which

$$k_1^o = \frac{1}{c_{55}^o} \begin{vmatrix} c_{55}^o & c_{56}^o \\ c_{56}^o & c_{66}^o \end{vmatrix} \ . \tag{32}$$

Simultaneous solution of (29c) and (29d) for e_3 and e_4 in terms of e_1 and e_2 permits one to write (29a) in the form

$$T_1^o = k_2^o e_1 + k_3^o e_2 \ , \tag{33}$$

where

$$k_2^o = N_2^o / D_{234}^o \ , \qquad k_3^o = N_3^o / D_{234}^o \ , \tag{34}$$

and

$$N_2^o = \begin{vmatrix} c_{11}^o & c_{13}^o & c_{14}^o \\ c_{13}^o & c_{33}^o & c_{34}^o \\ c_{14}^o & c_{34}^o & c_{44}^o \end{vmatrix} , \tag{35}$$

$$N_3^o = \begin{vmatrix} c_{12}^o & c_{23}^o & c_{24}^o \\ c_{13}^o & c_{33}^o & c_{34}^o \\ c_{14}^o & c_{34}^o & c_{44}^o \end{vmatrix} , \tag{36}$$

$$D_{234}^o = \begin{vmatrix} c_{33}^o & c_{34}^o \\ c_{34}^o & c_{44}^o \end{vmatrix} . \tag{37}$$

Similarly, Equation (29b) is written

$$T_2^o = k_3^o e_1 + k_4^o e_2 \quad , \tag{38}$$

where

$$k_4^o = N_4^o / D_{234}^o \quad , \tag{39}$$

$$N_4^o = \begin{vmatrix} c_{22}^o & c_{23}^o & c_{24}^o \\ c_{23}^o & c_{33}^o & c_{34}^o \\ c_{24}^o & c_{34}^o & c_{44}^o \end{vmatrix} \quad . \tag{40}$$

Equation (20), for the strain-energy-function W to be included in the variational equation (21), is reduced to the following expression in view of the assumptions under present consideration:

$$2W = T_1^o e_1 + T_2^o e_2 + T_6^o e_6 \quad .$$

Upon the introduction of (31), (33), and (38) into the above, we obtain

$$2W = k_2^o e_1^2 + 2k_3^o e_1 e_2 + k_4^o e_2^2 + k_1^o e_6^2 \quad . \tag{41}$$

In subsequent discussions, we will find that the following parameters play an important part in the mathematical development:

$$K_{(a)_1}^o = k_2^o / k_1^o = 2.7263 \quad , \tag{42}$$

$$K_{(a)_2}^o = k_3^o / k_1^o = -0.2044 \quad , \tag{43}$$

$$K_{(a)_3}^o = k_4^o / k_1^o = 4.4358 \quad , \tag{44}$$

where the numerical values have been determined by using the c_{pq}^o which are tabulated in Appendix B.

Set (b): $T_2^o = T_3^o = T_4^o = 0$ throughout the plate. Simultaneous solution of (29b) through (29d) yields e_2, e_3, and e_4 in terms of e_1. Substitution of these quantities into (29a) gives

$$T_1^o = k_5^o e_1 \quad , \tag{45}$$

in which

$$k_5^o = N_5^o / N_4^o \quad , \tag{46}$$

$$N_5^o = \begin{vmatrix} c_{11}^o & c_{12}^o & c_{13}^o & c_{14}^o \\ c_{12}^o & c_{22}^o & c_{23}^o & c_{24}^o \\ c_{13}^o & c_{23}^o & c_{33}^o & c_{34}^o \\ c_{14}^o & c_{24}^o & c_{34}^o & c_{44}^o \end{vmatrix} \quad , \tag{47}$$

and N_4^o is defined in Equation (40).

The assumptions of Set (b) are introduced into Equation (20) to give

$$2W = T_1^o e_1 + T_5^o e_5 + T_6^o e_6 \quad ,$$

or

$$2W = k_5^o e_1^2 + c_{55}^o e_5^2 + 2c_{56}^o e_5 e_6 + c_{66}^o e_6^2 \quad , \tag{48}$$

wherein Equations (29e), (29f), and (45) have been employed.

A parameter which proves significant in subsequent mathematical studies based on this subsection is

$$K_{(b)}^o = k_5^o / c_{66}^o = 2.7093 \quad . \tag{49}$$

The numerical value above is obtained by using the c_{pq}^o given in Table B-VII together with Equations (40), (46), and (47).

Mathematical models which have been studied in conjunction with the two sets of assumptions are presented next. The selection of a specific mathematical representation for the displacements permits one to express the strain-energy function explicitly in terms of position coordinates. Thereafter, the

variational problem of Equation (21) can be solved to determine resonant frequencies of vibration. Following the presentation of models, we will take Assumption Set (b) above in combination with one of the models and will display in detail the analytical procedures which yield resonant frequencies.

9. Mathematical Models

Several mathematical representations for the displacements $u(x,y,z,t)$, $v(x,y,z,t)$, and $w(x,y,z,t)$ along the respective axes x,y,z of Figure 2c were selected for analysis. These selections were based upon two separate facts. First, the frequencies associated with the coupled thickness-shear and flexure modes of interest appear to be essentially independent of the crystal's z_o-dimension; accordingly, we assumed

$$w(x,y,z,t) \equiv 0 \tag{50}$$

in all of the cases considered. Second, the frequencies associated with coupled thickness-shear and flexure vibrations of a finite plate (having width and length large compared to thickness) are predicted approximately by simple infinite-plate theory; therefore, to describe more accurately these vibration modes for the case of a finite plate, we can suitably modify the known infinite-plate results.

We first write the displacements u and v in the form

$$u(x,y,z,t) = \hat{u}(x,y,z) \sin \omega t \quad , \tag{51}$$

$$v(x,y,z,t) = \hat{v}(x,y,z) \sin \omega t \quad , \tag{52}$$

in which ω is the angular frequency of vibration. Next, we represent $\hat{u}$ and $\hat{v}$ in terms of known functions of y and arbitrary functions of x. The quantity η appearing in the representations is defined as

$$\eta = \frac{y}{y_o/2} \quad . \tag{53}$$

Listed below are the various model forms which have been considered. It may be noted--with reference to Forms (6), (7), and (8)--that the expression $\hat{u} = f(x) \sin (\frac{\pi}{2}\eta) + g(x) \sin^3(\frac{\pi}{2}\eta)$ is more readily treated when written in the entirely equivalent form $\hat{u} = f(x) \sin (\frac{\pi}{2}\eta) + g(x) \sin (3\frac{\pi}{2}\eta)$. Similarly, in place of $\hat{v} = \Phi(x) + \psi(x) \cos^2(\frac{\pi}{2}\eta)$ we would use $\hat{v} = \Phi(x) + \psi(x) \cos (2\frac{\pi}{2}\eta)$.

Form	$\hat{u}$ =	$\hat{v}$ =
(1)	$f(x) \sin(\frac{\pi}{2}\eta)$	$\Phi(x)$
(2)	$f(x) \sin(\frac{\pi}{2}\eta) + g(x)\,\eta$	$\Phi(x)$
(3)	$f(x) \sin(\frac{\pi}{2}\eta) + g(x)\,\eta + h(x)\,\eta^3$	$\Phi(x)$
(4)	$f(x) \sin(\frac{\pi}{2}\eta) + g(x)\,\eta$	$\Phi(x) + \psi(x)\,\eta^2$
(5)	$[f(x) + g(x)\,\eta^2] \sin(\frac{\pi}{2}\eta)$	$\Phi(x)$
(6)	$f(x) \sin(\frac{\pi}{2}\eta) + g(x) \sin^3(\frac{\pi}{2}\eta)$	$\Phi(x)$
(7)	$f(x) \sin(\frac{\pi}{2}\eta) + g(x) \sin^3(\frac{\pi}{2}\eta) + h(x) \sin^5(\frac{\pi}{2}\eta)$	$\Phi(x)$
(8)	$f(x) \sin(\frac{\pi}{2}\eta) + g(x) \sin^3(\frac{\pi}{2}\eta)$	$\Phi(x) + \psi(x) \cos^2(\frac{\pi}{2}\eta)$
(9)	$f(x) \sin(\frac{\pi}{2}\eta) + g(x) \sinh(m\eta)$, (m arbitrary)	$\Phi(x)$

The mathematical development now proceeds as follows. One set of assumptions in Section 8 is taken in conjunction with one of the above models, and the strain-energy-function is written as a function of x and y. The variational equation in (21) then yields an eigenvalue problem which may be solved for the corresponding eigenfrequencies. In the following section, these procedures are detailed for Assumption Set (b) and Model Form (3), the combination which has yielded a resonance chart quantitatively similar to that obtained experimentally. A criterion is established with which to assess various combinations of assumptions and models.

10. Analytical Development

The analysis resulting in resonant frequencies of vibration will here be detailed using Assumption Set (b) of Section 8, Model Form (3) of Section 9, and Equations (50) through (53). Reference to Equation (6) reveals that now $e_5 = 0$; hence the strain-energy-function of (48) assumes the form

$$2W = k_5^o e_1^2 + c_{66}^o e_6^2 \quad . \tag{54}$$

Substituting (54) into (21) and using (51) and (52), we obtain

$$\int_{-x_o/2}^{x_o/2} dx \int_{-y_o/2}^{y_o/2} dy \int_{-z_o/2}^{z_o/2} dz\ \delta[-\omega^2\rho(\hat{u}^2 + \hat{v}^2) + k_5^o e_1^2 + c_{66}^o e_6^2] = 0 \ . \qquad (55)$$

Integration with respect to z yields but a multiplicative constant. Using Model Form (3), we next integrate with respect to y and then perform the indicated variation. Thereupon, Equation (55) becomes

$$\int_{-x_o/2}^{x_o/2} [F\delta f + G\delta g + H\delta h + \Phi\delta\phi + \bar{F}\delta f' + \bar{G}\delta g' + \bar{H}\delta h' + \bar{\Phi}\delta\phi'] \, dx = 0 \ , \qquad (56)$$

where primes signify differentiation with respect to the variable x and the quantities designated by capital letters are defined as follows:

$$\begin{aligned}
F &= c_{66}^o[\beta^2(f + a_1 g + a_2 h) + \tfrac{4}{\pi}\beta\phi'] - \omega^2\rho(f + a_1 g + a_2 h) \ , \\
G &= c_{66}^o[a_1\beta^2(f + g + h) + \tfrac{4}{\pi}\beta\phi'] - \omega^2\rho(a_1 f + \tfrac{2}{3}g + \tfrac{2}{5}h) \ , \\
H &= c_{66}^o[\beta^2(a_2 f + a_1 g + \tfrac{9}{5}a_1 h) + \tfrac{4}{\pi}\beta\phi'] - \omega^2\rho(a_2 f + \tfrac{2}{5}g + \tfrac{2}{7}h) \ , \\
\Phi &= -2\omega^2\rho\phi \ ;
\end{aligned} \qquad (57a)$$

$$\begin{aligned}
\bar{F} &= k_5^o(f' + a_1 g' + a_2 h') \ , \qquad \bar{G} = k_5^o(a_1 f' + \tfrac{2}{3}g' + \tfrac{2}{5}h') \\
\bar{H} &= k_5^o(a_2 f' + \tfrac{2}{5}g' + \tfrac{2}{7}h') \ , \qquad \bar{\Phi} = c_{66}^o[\tfrac{4}{\pi}\beta(f + g + h) + 2\phi']
\end{aligned} \qquad (57b)$$

In the above

$$a_1 = 8/\pi^2 \ , \qquad a_2 = 3a_1(1 - a_1) \ , \qquad \beta = \pi/y_o \ . \qquad (58)$$

If one now integrates by parts the last four terms of Equation (56)—for example,

$$\int_{-x_o/2}^{x_o/2} \bar{F}\delta f' \, dx = \left[\bar{F}\delta f\right]_{-x_o/2}^{x_o/2} - \int_{-x_o/2}^{x_o/2} \frac{d\bar{F}}{dx}\,\delta f \, dx \ ,$$

one obtains the following differential equations

$$\begin{aligned} F - d\bar{F}/dx = 0 \ , \qquad & G - d\bar{G}/dx = 0 \ , \\ H - d\bar{H}/dx = 0 \ , \qquad & \Phi - d\bar{\Phi}/dx = 0 \ , \end{aligned} \tag{59}$$

together with the natural boundary conditions

$$\bar{F} = \bar{G} = \bar{H} = \bar{\Phi} = 0 \quad \text{at } x = \pm x_o/2 \ . \tag{60}$$

A solution of (59) is obtained by assuming that

$$\begin{aligned} f(x) = A \cos \alpha x \ , \qquad & g(x) = B \cos \alpha x \ , \\ h(x) = C \cos \alpha x \ , \qquad & \varphi(x) = D \sin \alpha x \ , \end{aligned} \tag{61}$$

in which A, B, C, D, and α are constants. Introduction of (61) into (59) results in

$$\begin{aligned} &[1]A + [7]B + [6]C + [5]D = 0 \ , \\ &[7]A + [2]B + [8]C + [5]D = 0 \ , \\ &[6]A + [8]B + [3]C + [5]D = 0 \ , \\ &[5]A + [5]B + [5]C + [4]D = 0 \ , \end{aligned} \tag{62}$$

where

$$\begin{aligned} [1] &= [K^{o}_{(b)}\bar{y} - \bar{x}] + 1 \ , & [5] &= \sqrt{2a_1\bar{y}} \ , \\ [2] &= \tfrac{2}{3}[K^{o}_{(b)}\bar{y} - \bar{x}] + a_1 \ , & [6] &= a_2[1] \ , \\ [3] &= \tfrac{2}{7}[K^{o}_{(b)}\bar{y} - \bar{x}] + \tfrac{9}{5}a_1 \ , & [7] &= a_1[1] \ , \\ [4] &= 2(\bar{y} - \bar{x}) \ , & [8] &= \tfrac{2}{5}[K^{o}_{(b)}\bar{y} - \bar{x}] + a_1 \ , \end{aligned} \tag{63}$$

and

$$\bar{x} = \frac{\omega^2\rho}{c^{o}_{66}\beta^2} = \frac{\omega^2}{\omega_o^2} \ , \qquad \bar{y} = \alpha^2/\beta^2 \ ; \text{ also,} \tag{64}$$

the parameter $K^{o}_{(b)}$ is defined in (49) and ω_o represents the angular vibration frequency for a quartz plate of thickness y_o and unbounded length and width.

Nontrivial solutions exist for the set (62) provided that the secular determinant of the equations vanishes. Thus one obtains the constant $\bar{y}$, or α through a relation in (64), as a function of $\bar{x}$. Corresponding to each value of $\bar{x}$ are four real values of $\bar{y}$ ($\bar{y}_1 > \bar{y}_2 > \bar{y}_3 > \bar{y}_4$). For $\bar{x} = 1$, $\bar{y}_2 = 0$. The solutions (61) consequently assume the complete form

$$\left.\begin{aligned} f(x) &= A_j \cos \alpha_j x \quad , \\ g(x) &= B_j \cos \alpha_j x \quad , \\ h(x) &= C_j \cos \alpha_j x \quad , \\ \Phi(x) &= D_j \sin \alpha_j x \quad . \end{aligned}\right\} \qquad (j = 1 \text{ to } 4) \qquad (65)$$

Equations (62) can now be solved simultaneously for the ratios B_j/A_j, C_j/A_j, D_j/A_j ($j = 1$ to 4).

Finally, the coefficients A_j are determined by invoking the boundary conditions (60). These can be written as

$$\left.\begin{aligned} f' = g' = h' &= 0 \\ \frac{2\beta}{\pi}(f + g + h) + \Phi' &= 0 \end{aligned}\right\} \qquad \text{at } x = \pm x_o/2 \quad . \qquad (66)$$

The first relation of (66) gives, with the aid of (65),

$$\left.\begin{aligned} A_j\sqrt{\bar{y}_j}\ \sin(\tfrac{\pi}{2}\nu_j) &= 0 \quad , \\ A_j(\tfrac{B_j}{A_j}\sqrt{\bar{y}_j}\ \sin(\tfrac{\pi}{2}\nu_j) &= 0 \quad , \\ A_j(\tfrac{C_j}{A_j}\sqrt{\bar{y}_j}\ \sin(\tfrac{\pi}{2}\nu_j) &= 0 \quad , \end{aligned}\right\} \qquad (67)$$

where

$$\nu_j = \sigma\sqrt{\bar{y}_j} \quad , \qquad \sigma = x_o/y_o \quad . \qquad (68)$$

The second equation in (66) is transformed as follows using the fourth relation of (62) together with Equations (65):

$$A_j\left(\frac{D_j}{A_j}\right)\frac{1}{\sqrt{\bar{y}_j}}\cos\left(\frac{\pi}{2}\nu_j\right) = 0 \quad . \tag{69}$$

In order for the set consisting of (67) and (69) to have nontrivial solutions,

$$\begin{vmatrix} 1 & 1 & 1 & 1 \\ B_1/A_1 & B_2/A_2 & B_3/A_3 & B_4/A_4 \\ C_1/A_1 & C_2/A_2 & C_3/A_3 & C_4/A_4 \\ J_1D_1/A_1 & J_2D_3/A_2 & J_3D_3/A_3 & J_4D_4/A_4 \end{vmatrix} = 0 \tag{70}$$

in which

$$J_m = \frac{1}{\sqrt{\bar{y}_m}}\cot\left(\frac{\pi}{2}\nu_m\right) \quad , \qquad \text{(no summation; } m = 1, 2, 3, 4) \; . \tag{71}$$

Solution of (70) determines an infinite set of σ values corresponding to given $\bar{x}$. This means that the ratio ω/ω_o of eigenfrequencies has been found for any specified ratio x_o/y_o of length/thickness. Equation (70) is inapplicable when $\bar{x} = 1$, for which $\bar{y}_2 = 0$. However, the set (67) remains valid in this case and one finds immediately that

$$\sigma(1) = \frac{2n}{\sqrt{\bar{y}_1(1)}} \quad , \tag{72}$$

where n is an integer.

It is noted that adjacent $\sigma(1)$ values are spaced by the amount

$$\Delta\sigma(1) = \frac{2}{\sqrt{\bar{y}_1(1)}} \quad . \tag{73}$$

This spacing provides a convenient criterion with which to assess the various assumptions and models cited earlier. For an $\bar{x}$ of unity, we obtain the root $\bar{y}_1(1)$ of the secular determinant (62) with but a moderate amount of computation.

The following section contains a tabulation of $\Delta\sigma(1)$ as calculated for various combinations of the assumption sets and model forms of Sections 8 and 9. In each case the analytical procedures are similar to those outlined in the present section. However, when Assumption Set (a) is used, the constant $K^{o}_{(a)_1}$ defined by (42) appears in place of $K^{o}_{(b)}$ and the parameters $K^{o}_{(a)_2}$ and $K^{o}_{(a)_3}$ of Equations (43) and (44) play a role.

11. Tabulation of Results

The foregoing analysis is typical of that encountered when studying a model form of Section 9 in conjunction with one of the assumption sets in Section 8. A secular determinant always results and is similar to that obtained from Equations (62). For every combination of assumption set and model form, solution of the corresponding secular equation at $\bar{x} = 1$ gives $\bar{y}_2(1) = 0$. Moreover, $y_3(1)$, $\bar{y}_4(1), \ldots y_q(1)$, where q = the number of x-functional coefficients (f, g, h, φ, ψ) involved, are found to be relatively large negative numbers. For those roots which are negative, the trigonometric cotangent function appearing in the secular equation corresponding to (70) can be transformed into a hyperbolic cotangent function. Since $\sigma \gg 1$, all hyperbolic cotangent functions are approximately unity. At $\bar{x} = 1$, then, the secular equation for the determination of σ has in every instance the general solution

$$\sigma(1) = \frac{2n}{\sqrt{\bar{y}_1(1)}} + \mathfrak{F}[\bar{y}_1(1), \bar{y}_3(1), \ldots \bar{y}_q(1)] \quad , \tag{74}$$

where the function $\mathfrak{F}$ does not contain the integer n. Thus, we associate with each combination of assumption and model the separation in adjacent eigenvalues at $\bar{x} = 1$ which is expressed in Equation (73).

Table I contains values for $\Delta\sigma(1)$ corresponding to the various combinations of assumption sets and model forms which we have thus far exploited. An entry under "Model" designates by letter the pertinent assumption set and by numeral the mathematical model form which was utilized. For example, Model b3 in Table I refers to the association of Assumption Set (b) with Model Form (3), the case in which we examined in some detail in Section 10. It is noted that Model a9 contains an arbitrary constant m. The value m = 2 which was selected for presentation in Table I is one which leads to an eigenvalue spacing in keeping with the experimental result. Of course, m can be chosen so as to assure that $\Delta\sigma(1)$

will conform exactly to the experimental findings.

Table I. Separation in Adjacent Eigenvalues at $\bar{x} = 1$.

Model	$\Delta\sigma(1)$	Model	$\Delta\sigma(1)$
a1	1.7559	a7	1.6931
a2	1.6115	a8	1.6686
a3	1.6091	a9	1.6096 ($m = 2$)
a4	1.6048	b1	1.7547
a5	1.4673	b2	1.6102
a6	1.6945	b3	1.6078

From an examination of experimental resonant frequencies recently obtained by Koga [5] for coupled thickness-shear and flexure vibration modes of rectangular, quartz crystals, we have concluded that Model b3 provides us with a more favorable agreement between theory and experiment than that realized with the other models which were studied. Although Model a9 can be made to yield an eigenvalue spacing in exact agreement with that determined experimentally, we have avoided this model on the basis that inclusion in the theory of an arbitrary constant lacks rigor. It is recalled that Mindlin has incorporated such an adjustable constant in his description of the vibrating crystal plate.

12. Conclusion

In review, we will summarize the assumptions which constitute Model b3 and restate the mathematical description applying in this case. Stresses T_2^o, T_3^o, and T_4^o are assumed to be negligible throughout the rectangular plate--that is, tension stresses on planes perpendicular to the y-axis and z-axis (see Figure 2c) and the y-component of shear on planes perpendicular to the z-axis are regarded as inconsequential. Displacements u, v, and w along the coordinate axes x, y, and z, respectively, are taken as

$$u(x,y,z,t) = [f(x)\,\sin(\tfrac{\pi}{2}\eta) + g(x)\,\eta + h(x)\,\eta^3]\,\sin\omega t \quad ,$$

$$v(x,y,z,t) = \phi(x)\,\sin\omega t \quad , \qquad w(x,y,z,t) = 0 \quad ,$$

where η is defined by Equation (53) and the functions of x by (65).

A complete analytical treatment of Model b3 is contained in Section 10. Length/thickness ratios σ for various normalized frequencies ω/ω_o $(= \sqrt{\bar{x}})$ were found from Equation (70) with the aid of the Burroughs 220 Digital Calculator of Georgia Tech's Rich Electronic Computer Center. Since our present interest centers on the vicinity of the fundamental high-frequency shear vibration, only the neighborhood of $\bar{x} = 1$ was investigated. Figure 3 is a chart of the computed resonant frequencies associated with Model b3 and incorporates for comparison some of the experimental results determined by Koga [5]. As anticipated, we observe an especially good agreement between theoretical and experimental values in the immediate vicinity of $\bar{x} = 1$.

If $\bar{x}$ is but slightly larger than unity, Equation (70) has an approximate solution which is readily determined. First, we expand (70) to read

$$S_i J_i D_i / A_i = 0 \quad , \qquad (i = 1 \text{ to } 4) \qquad (75)$$

where S_i signifies the cofactor obtained by deleting the bottom row and the i-th column from the determinant in (70). For $\bar{x}$ values which are slightly larger than unity, the third and fourth terms in (75) are found to be negligibly small throughout the range of σ depicted in Figure 3. Equation (70) can thus be replaced by the approximate expression

$$S_1 J_1 D_1 / A_1 + S_2 J_2 D_2 / A_2 = 0 \quad . \qquad (76)$$

A solution of (76) is that for which ν_1 and ν_2 are both odd integers. The corresponding values of σ approximately specify, in the region above $\omega/\omega_o = 1$ in Figure 3, particular points of inflection. The locus of inflection points for which $\nu_2 = 1$ very nearly depicts the relationship between resonant frequency and length/thickness ratio for the circumstance of a rectangular, AT-cut plate vibrating in the fundamental thickness-shear mode (see Figure 1b). Similarly, we associate the locus of points for which $\nu_2 = 3$ with the third inharmonic thickness-shear vibration, etc. An approximate equation may be derived for these loci, as follows: Since the curve of $\bar{y}_2(\bar{x})$ versus $\bar{x}$ is practically linear near $\bar{x} = 1$, we can represent this portion of the curve by the relationship

$$\bar{x} - 1 = \bar{y}_2 \, [d\bar{x}/d\bar{y}_2]_{\bar{x}=1} = \bar{y}_2 \, [K^o_{(b)} + a_1] \quad , \qquad (77)$$

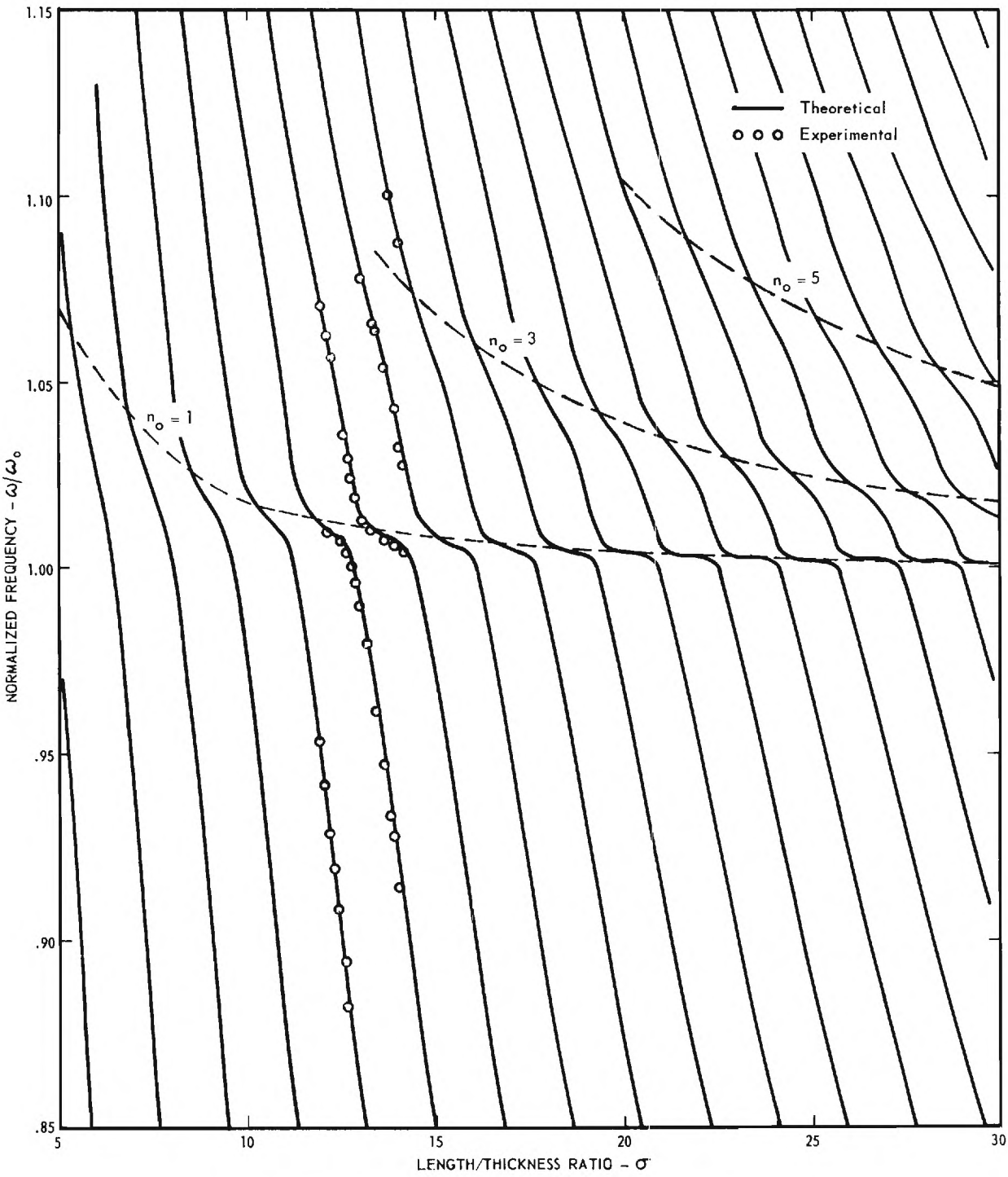

Figure 3. Normalized Frequency Versus Length/Thickness Ratio for Coupled Thickness-Shear and Flexural Vibrations of Rectangular, AT-Cut Quartz Plates of Constant Width.

where $K^{o}_{(b)}$ is given by Equation (49) and a_1 is defined in (58). Multiplying both sides of (77) by σ^2 and replacing $\sigma\sqrt{\bar{y}}_2$ ($= \nu_2$) by an odd integer n_o, we have

$$(\bar{x} - 1)\,\sigma^2 = n_o^2\,[K^{o}_{(b)} + a_1] \tag{78}$$

in which $n_o = 1$ represents the fundamental thickness-shear mode, $n_o = 3$ its third inharmonic, etc. Plots of Equation (78) for $n_o = 1$, 3, and 5 are displayed in Figure 3 as dashed-line curves.

For additional discussion relating to the resonance chart of Figure 3, the reader is referred to the paper by Koga [5]. This publication includes a brief resume of the laboratory arrangement that was employed to obtain the experimental data which is plotted in Figure 3. Detailed information concerning the experimental program is to be found in References [9] and [14]. It may be mentioned that Koga has found a close agreement between the polarization distributions as computed using Model b3 and those which he obtained experimentally, a result that is included in Reference [5].

Recent theoretical investigations by Mindlin [15,16] have resulted in resonant frequencies which match in much detail early experimental data obtained by Koga and Fukuyo [2]. Extensional modes are included together with flexure and thickness-shear deformations. Mindlin's latest theoretical model lacks the refinement which one finds in the present analysis; his approach is again by way of differential equations of motion and neglects entirely any piezoelectric effects. As in Reference [4], he introduces arbitrary constants to compensate in part for the omission of higher-order terms in y as far as displacements are concerned. In short, if the extensional deformation is suppressed, Mindlin's recent effort reduces to that contained in Reference [3] with an additional degree of mathematical refinement, and is therefore in effect similar to his approach which we outlined in Section 6. In comparing his recent theory with experimental data, Mindlin employs a set of elastic constants several of which differ by as much as 1% from those reported by Koga et al [13] and utilized in the present analysis.

APPENDIX A

TRANSFORMATION OF CONSTANTS

As noted in the text, the elastic, piezoelectric, and dielectric stiffness constants involved in the theoretical analysis are based on the xyz-coordinate system of Figure 2c. Numerical values for these constants are tabulated in the following appendix and are based on measurements made by Koga et al [13]. The latter experimental data were taken with respect to the crystallographic axes X,Y,Z of quartz shown in Figure 2a. Reference to Figure 2b reveals that the problem coordinate system is rotated counterclockwise about the X-crystallographic axis by the angle $(\frac{\pi}{2} - \theta)$.

The present appendix contains the transformation relations required to obtain the elastic, piezoelectric, and dielectric stiffness constants appropriate to the problem coordinate system, having given their counterparts as measured along the crystallographic axes. All quantities referring to the latter axes are primed, while unprimed constants refer to the xyz-coordinate system. The rotation angle is that given by the approximation of Equation (1), while the transformation equations are those of Sykes [12].*

$$c_{11} = c'_{11}$$

$$c_{12} = \frac{2}{3}c'_{12} + \frac{1}{3}c'_{13} + \frac{2\sqrt{2}}{3}c'_{14}$$

$$c_{13} = \frac{1}{3}c'_{12} + \frac{2}{3}c'_{13} - \frac{2\sqrt{2}}{3}c'_{14}$$

$$c_{14} = -\frac{\sqrt{2}}{3}c'_{12} + \frac{\sqrt{2}}{3}c'_{13} + \frac{1}{3}c'_{14}$$

$$c_{22} = \frac{4}{9}c'_{11} + \frac{4}{9}c'_{13} - \frac{8\sqrt{2}}{9}c'_{14} + \frac{1}{9}c'_{33} + \frac{8}{9}c'_{44}$$

$$c_{23} = \frac{2}{9}c'_{11} + \frac{5}{9}c'_{13} + \frac{2\sqrt{2}}{9}c'_{14} + \frac{2}{9}c'_{33} - \frac{8}{9}c'_{44}$$

$$c_{24} = -\frac{2\sqrt{2}}{9}c'_{11} + \frac{\sqrt{2}}{9}c'_{13} + \frac{2}{9}c'_{14} + \frac{\sqrt{2}}{9}c'_{33} + \frac{2\sqrt{2}}{9}c'_{44}$$

$$c_{33} = \frac{1}{9}c'_{11} + \frac{4}{9}c'_{13} + \frac{4\sqrt{2}}{9}c'_{14} + \frac{4}{9}c'_{33} + \frac{8}{9}c'_{44}$$

$$c_{34} = -\frac{\sqrt{2}}{9}c'_{11} - \frac{\sqrt{2}}{9}c'_{13} - \frac{5}{9}c'_{14} + \frac{2\sqrt{2}}{9}c'_{33} - \frac{2\sqrt{2}}{9}c'_{44}$$

---

* Sykes' angle θ corresponds in our notation to $(\frac{\pi}{2} + \theta)$.

$$c_{44} = \frac{2}{9}c'_{11} - \frac{4}{9}c'_{13} + \frac{2\sqrt{2}}{9}c'_{14} + \frac{2}{9}c'_{33} + \frac{1}{9}c'_{44}$$

$$c_{55} = -\frac{2\sqrt{2}}{3}c'_{14} + \frac{2}{3}c'_{44} + \frac{1}{3}c'_{66}$$

$$c_{56} = \frac{1}{3}c'_{14} + \frac{\sqrt{2}}{3}c'_{44} - \frac{\sqrt{2}}{3}c'_{66}$$

$$c_{66} = \frac{2\sqrt{2}}{3}c'_{14} + \frac{1}{3}c'_{44} + \frac{2}{3}c'_{66}$$

$$\varepsilon_{11} = \varepsilon'_{11}$$

$$\varepsilon_{12} = -\frac{2}{3}\varepsilon'_{11} + \frac{2\sqrt{2}}{3}\varepsilon'_{14}$$

$$\varepsilon_{13} = -\frac{1}{3}\varepsilon'_{11} + \frac{2\sqrt{2}}{3}\varepsilon'_{14}$$

$$\varepsilon_{14} = \frac{\sqrt{2}}{3}\varepsilon'_{11} + \frac{1}{3}\varepsilon'_{14}$$

$$\varepsilon_{25} = \frac{\sqrt{2}}{3}\varepsilon'_{11} - \frac{2}{3}\varepsilon'_{14}$$

$$\varepsilon_{26} = -\frac{2}{3}\varepsilon'_{11} - \frac{\sqrt{2}}{3}\varepsilon'_{14}$$

$$\varepsilon_{35} = -\frac{1}{3}\varepsilon'_{11} + \frac{\sqrt{2}}{3}\varepsilon'_{14}$$

$$\varepsilon_{36} = \frac{\sqrt{2}}{3}\varepsilon'_{11} + \frac{1}{3}\varepsilon'_{14}$$

$$\gamma_{11} = \gamma'_{11}$$

$$\gamma_{22} = \frac{2}{3}\gamma'_{11} + \frac{1}{3}\gamma'_{33}$$

$$\gamma_{23} = -\frac{\sqrt{2}}{3}(\gamma'_{11} - \gamma'_{33})$$

$$\gamma_{33} = \frac{1}{3}\gamma'_{11} + \frac{2}{3}\gamma'_{33}$$

APPENDIX B

TABULATION OF NUMERICAL CONSTANTS

This appendix contains numerical values for the various physical constants involved in the theoretical analysis. Elastic, piezoelectric, and dielectric stiffness constants as measured by Koga et al [13] along the crystallographic axes of quartz (at 20°C) are denoted by primes and tabulated first. Next, the corresponding quantities (unprimed) as referred to the rotated coordinate system of Figure 2c are given. These latter values are obtained from the previous experimental data by means of the transformation equations in Appendix A, where the rotation angle has been taken as that given by Equation (1). Lastly, numerical values are cited for the elastopiezoelectric coefficients defined in Equation (30). Since all elastic and piezoelectric quantities were measured with respect to the density ρ as a basis, we define $\tilde{c}_{mn} = c_{mn}/4\rho$ and $\tilde{\varepsilon}_{mn} = \varepsilon_{mn}/\sqrt{4\rho}$. All tabulated values have the units indicated, and any quantity not listed has the value zero.

Table B-I. Experimental Elastic Constants as Measured Along the Crystallographic Axes of Quartz. Units: $10^{10}\text{cm}^2\text{sec}^{-2}$

$\tilde{c}'_{11} = 8.1957$	$\tilde{c}'_{12} = 0.6693$	$\tilde{c}'_{13} = 1.1264$
$\tilde{c}'_{14} = -1.7050$	$\tilde{c}'_{22} = 8.1957$	$\tilde{c}'_{23} = 1.1264$
$\tilde{c}'_{24} = 1.7050$	$\tilde{c}'_{33} = 9.9990$	$\tilde{c}'_{44} = 5.4986$
$\tilde{c}'_{55} = 5.4986$	$\tilde{c}'_{56} = -1.7050$	$\tilde{c}'_{66} = 3.7632$.

Table B-II. Experimental Piezoelectric Constants as Measured Along the Crystallographic Axes of Quartz. Units: 10^4 esu sec^{-1} $dyne^{-1/2}$

$\tilde{\varepsilon}'_{11} = -1.6129$	$\tilde{\varepsilon}'_{14} = 0.3748$
$\tilde{\varepsilon}'_{12} = 1.6129$	$\tilde{\varepsilon}'_{25} = -0.3748$
$\tilde{\varepsilon}'_{26} = 1.6129$	

Table B-III. Experimental Dielectric Stiffness Constants as Measured Along the Crystallographic Axes of Quartz. Units: erg cm esu^{-2}

$\gamma'_{11} = 2.7981$	$\gamma'_{22} = 2.7981$	$\gamma'_{33} = 2.7318$

Table B-IV. Elastic Constants Applicable to the Coordinate System of Figure 2c. Units: 10^{10} cm^2 sec^{-2}

$\tilde{c}_{11} = 8.1957$	$\tilde{c}_{12} = -0.7858$	$\tilde{c}_{13} = 2.5815$
$\tilde{c}_{14} = -0.3529$	$\tilde{c}_{22} = 12.2851$	$\tilde{c}_{23} = -0.7544$
$\tilde{c}_{24} = 0.5217$	$\tilde{c}_{33} = 9.6712$	$\tilde{c}_{34} = 0.8967$
$\tilde{c}_{44} = 3.6178$	$\tilde{c}_{55} = 6.5276$	$\tilde{c}_{56} = 0.2497$
	$\tilde{c}_{66} = 2.7342$	

Table B-V. Piezoelectric Constants Applicable to the Coordinate System of Figure 2c. Units: 10^4 esu sec^{-1} $dyne^{-1/2}$

$\tilde{\varepsilon}_{11} = -1.6129$	$\tilde{\varepsilon}_{25} = -1.0101$
$\tilde{\varepsilon}_{12} = 1.4286$	$\tilde{\varepsilon}_{26} = 0.8986$
$\tilde{\varepsilon}_{13} = 0.1843$	$\tilde{\varepsilon}_{35} = 0.7143$
$\tilde{\varepsilon}_{14} = -0.6353$	$\tilde{\varepsilon}_{36} = -0.6353$

Table B-VI. Dielectric Stiffness Constants Applicable to the Coordinate System of Figure 2c. Units: erg cm esu^{-2}

$\gamma_{11} = 2.7981$	$\gamma_{23} = -0.0313$
$\gamma_{22} = 2.7760$	$\gamma_{33} = 2.7539$

Table B-VII. Elasto-Piezoelectric Coefficients. Units: 10^{10} cm^2 sec^{-2}

$\tilde{c}^o_{11} = 8.2685$	$\tilde{c}^o_{12} = -0.8503$	$\tilde{c}^o_{13} = 2.5732$
$\tilde{c}^o_{14} = -0.3242$	$\tilde{c}^o_{22} = 12.3422$	$\tilde{c}^o_{23} = -0.7470$
$\tilde{c}^o_{24} = 0.4963$	$\tilde{c}^o_{33} = 9.6722$	$\tilde{c}^o_{34} = 0.8934$
$\tilde{c}^o_{44} = 3.6291$	$\tilde{c}^o_{55} = 6.5562$	$\tilde{c}^o_{56} = 0.2243$
	$\tilde{c}^o_{66} = 2.7568$	

BIBLIOGRAPHY

1. I. Koga, Physics 3, 70 (1932)
2. I. Koga and H. Fukuyo, J. Inst. Elec. Comm. Engrs. Japan 36, 59 (1953)
3. R. D. Mindlin, J. Appl. Phys. 22, 316 (1951)
4. R. D. Mindlin, J. Appl. Phys. 23, 83 (1952)
5. I. Koga, To be published
6. W. P. Mason, Piezoelectric Crystals and Their Application to Ultrasonics, D. Van Nostrand Co., New York, 1950
   (a) p. 39
   (b) p. 27
7. W. G. Cady, Piezoelectricity, McGraw-Hill Book Co., New York, 1946
   (a) p. 183
   (b) p. 44
   (c) p. 163
   (d) p. 187
   (e) p. 166
8. R. D. Mindlin, An Introduction to the Mathematical Theory of Vibrations of Elastic Plates, U. S. Army Signal Corps Engineering Laboratories, Fort Monmouth, New Jersey, 1955, p. 1.11
9. I. Koga, et al, Quarterly Report No. 1 on Signal Corps Contract DA-36-039 SC-78910, Engineering Experiment Station, Georgia Institute of Technology, Atlanta, 1 August to 1 November 1958
   (a) p. 78
   (b) p. 81
10. A. E. H. Love, A Treatise on the Mathematical Theory of Elasticity, Dover Publications, New York, 1944
    (a) p. 166
    (b) p. 95
    (c) p. 100
    (d) p. 167
11. R. A. Sykes, B.S.T.J. 23, 52 (1944)
12. R. A. Heising, Quartz Crystals for Electrical Circuits, D. Van Nostrand Co., New York, 1946, p. 247
13. I. Koga, et al, Phys. Rev. 109, 1467 (1958)
14. I. Koga, et al, Final Report on Signal Corps Contract DA-36-039 SC-78905, Engineering Experiment Station, Georgia Institute of Technology, Atlanta, 1 March 1959 to 30 June 1960
15. R. D. Mindlin, Quart. Appl. Math. 19, 51 (1961)
16. R. D. Mindlin and D. C. Gazis, Final Report on Signal Corps Contract DA-36-039 SC-87414, Dept. of Civil Engineering and Engineering Mechanics, Columbia University, New York, 30 June 1961

FINAL REPORT

PROJECT B-214

MODES OF VIBRATION OF PIEZOELECTRIC QUARTZ CRYSTALS

ARTHUR L. BENNETT

Research Grant NSF-G18972

1 July 1961 to 30 September 1963

Prepared for
National Science Foundation
Washington, D. C.

Engineering Experiment Station
GEORGIA INSTITUTE OF TECHNOLOGY
Atlanta, Georgia

ENGINEERING EXPERIMENT STATION
GEORGIA INSTITUTE OF TECHNOLOGY
ATLANTA, GEORGIA

ANNUAL REPORT
PROJECT NO. B-214

MODES OF VIBRATION OF PIEZOELECTRIC QUARTZ CRYSTALS

By

Arthur L. Bennett

NATIONAL SCIENCE FOUNDATION
WASHINGTON, D. C.
RESEARCH GRANT NSF-G18972

1 JULY 1961 TO 30 JUNE 1962

ANNUAL REPORT

PROJECT NO. B-214

RESEARCH GRANT NSF-G18972

MODES OF VIBRATION OF PIEZOELECTRIC QUARTZ CRYSTALS

By Arthur L. Bennett

Engineering Experiment Station
Georgia Institute of Technology
Atlanta, Georgia

The purpose of this research is the measurement, analysis, and prediction of the modes of vibration of quartz peizoelectric crystals.

Background

The program for the two-year period covered by this NSF grant is a continuation of the work started in 1958 under the sponsorship of the U. S. Army Signal Research and Development Laboratories. Support was provided during 1960-61 under Grant NSF-G13647.

Prior to this undertaking only a limited number of measurements of the frequencies of response of quartz crystals to exciting frequencies other than the fundamental and overtones of the thickness-shear mode had been published.

An extensive series of theoretical papers by Mindlin and associates are available on the theoretical prediction of the frequencies of vibration of the various modes which can be excited by radio frequency applied to surface electrodes on the crystal. That work, as well as the early approximations by Koga, was based on the differential equations governing the motion of the crystal. The latest paper by Mindlin[1*] provides an excellent representation of the measurements by Fukuyo.[2] The theory does not include, however, the effect of piezo-

---

* Superscript numbers refer to references listed in Bibliography.

electric stiffness and arbitrary constants are introduced to compensate in part for the omission of higher-order terms dependent on the thickness. The elastic constants used in the computation were derived from the experimental data to be fitted. These constants differ as much as one per cent from those reported by Koga.[3]

Research Progress

Experimental. The measurement equipment and procedure previously described[4] have been extended to cover responses from 100 kc to 1100 kc as well as in the range 2700 kc to 3300 kc in the vicinity of the third overtone. During the year, 463 reductions averaging 10 microns each were made in the x dimension of the crystal. The frequencies of the significant responses are indicated in Figures 1 through 8.* The size of the dot is an indication of the strength of the response.

At intervals of about 0.5 mm, polarization recordings in both the x and z directions have been recorded for thirty or more of the stronger responses as an aid in identifying the mode of vibration at that response frequency.

During the year, equipment has been constructed for obtaining X-ray diffraction topographs of typical AT-cut quartz crystals by Lang's technique.[5] The effectiveness of this technique in showing imperfections (even individual dislocations) is striking. Furthermore, topographs taken with the (110) reflection for which the diffraction vector lies in the plane of the crystal plate show strongly the pattern of the flexure mode in agreement with the polarization records. This mode is coupled mechanically to the shear mode which is excited by the electrodes on the faces of the plate.

*The frequency scale (ordinate) of Figure 1 of the Final Report, Project No. B-185, Grant NSF-G13647, should be increased by 10 kc.

Preliminary experiments with narrow slits which confine the effective diffracting area of the crystal to a small volume relative to the thickness show promise of providing a measure of the variation of the strain amplitude in the thickness direction at a chosen x, z coordinate of the plate. This measurement has not heretofore been made to our knowledge.

Theoretical. The manuscript for the theory based on the variational approach has been completed and submitted to the Physical Review. Computer programs, run both at Georgia Tech and at Tokyo University, show excellent agreement of the computed values of the response frequencies. Comparison has been made both with the Georgia Tech measurements for the x dimension 10 to 15 times the thickness and also with Dr. Fukuyo's measurements[2] for a ratio of about 40. The coupled vibrations in thickness-shear and flexure of a rectangular AT-cut plate in the vicinity of the fundamental thickness-shear mode are treated. A plot of the predicted responses with the same measured values superposed has been forwarded in an Interim Report.[6] This report provides a discussion of the mathematical models considered in initiating the computer program. Figure 3 of the report is based on Model b3. Preliminary results of computation based on Model a4 indicate no significant change in the computed values.

Personnel

Dr. Koga spent July and part of August 1961 at Georgia Tech. With him came Masahiro Toki, graduate student at Yokohama National University, for a year on the project. Mr. Toki has continued the measurements of crystal D-1 with diligence and efficiency.

Dr. G. C. Knollman left Georgia Tech for industrial employment. His departure has delayed the planned theoretical investigations.

During the latter part of the year Mr. N. K. N. Hearn, Jr., under the guidance of Dr. R. A. Young, has spent a majority of his time on the development of the X-ray diffraction topography equipment and techniques.

Mr. J. I. Cochran has worked half-time beginning in April. He received the BEE degree in June and will be full-time on the project and part-time in EE graduate school.

The principal investigator has arranged relief from other responsibilities so that he can devote more time to the project during the second year of the grant.

Planned Work

The extension of the theory to the third overtone region of the rectangular crystal appears to be straight-forward and is being done. Exploratory work as a basis for a theory of the circular crystal is planned, but completion within the year is unlikely.

When the preferred mathematical model for the rectangular crystal has been selected, polarization patterns will be computed for comparison with the records of crystal D-1 made during the past year as well as for the added measurements planned during the coming year.

Additional rectangular crystals are being purchased for check measurements both by electrical and X-ray techniques. In addition to the natural quartz specimens, synthetic quartz rectangles will be measured. The work of King[7] at Bell Telephone Laboratories has indicated the need for careful attention to the anelastic characteristics of synthetic quartz.

The X-ray diffraction topographic technique is a powerful tool for the exploration of quartz crystals in oscillation. The polarization records indicate the average strain through the thickness (y-dimension) of the crystal at

a point. From traverses of the crystal in the x-direction at increments of z, a topograph of the polarization could be reconstructed. With the topographic photograph, however, a full map of the x-z plane is obtained at once. When wide slits are used, the topograph represents the effect of strain averaged through the thickness of the crystal, possibly more or less confused by the averaging of out-of-phase cells of the crystal along the incoming beam. At the expense of increased exposure time, narrow slits may be used. In this case the diffraction effects of a thin x, z layer of the crystal may be investigated as a function of y.

A further possibility which will be examined is the feasibility of synchronizing the X-ray emission with a particular phase of the oscillation of the crystal so that a stroboscopic exploration of the strain effects with phase may be made.

The techniques being developed will be applied to the evaluation of the interaction of the various modes of vibration with extended imperfections.

BIBLIOGRAPHY

1. R. B. Mindlin and D. C. Gazis, "Strong Resonances of Rectangular AT-cut Quartz Plates." Contracts Nonr-266(09) and Signal Corps Contracts DA36-039 SC-87414, July 1961.

2. Hitohiro Fukuyo, Bulletin of the Tokyo Institute of Technology, Series A, 1955, No. 1.

3. I. Koga, et al., Phys. Rev. 109, 1467 (1958).

4. Modes of Vibration of Piezoelectric Quartz Crystals. Final Report, Project No. B-185, Grant NSF G-13647, June 1961.

5. A. R. Lang, "Studies of Individual Dislocations in Crystals by X-Ray Diffraction Microradiography." J. Appl. Phys. 30, 1748 (Nov. 1959).

6. Coupled Thickness-Shear and Flexure Vibrations in Rectangular AT-cut at Quartz Plates. Interim Technical Report No. 1, Project No. B-214, March, 1962.

7. J. C. King, Fundamental Studies of the Properties of Natural and Synthetic Quartz Crystals. Final Report, Contract DA 36-039 SC-64586, June 1960; Final Report, Contract DA 36-039 SC-85364, August 1961; Third Interim Report, Contract DA 36-039 SC-87459, May 1962.

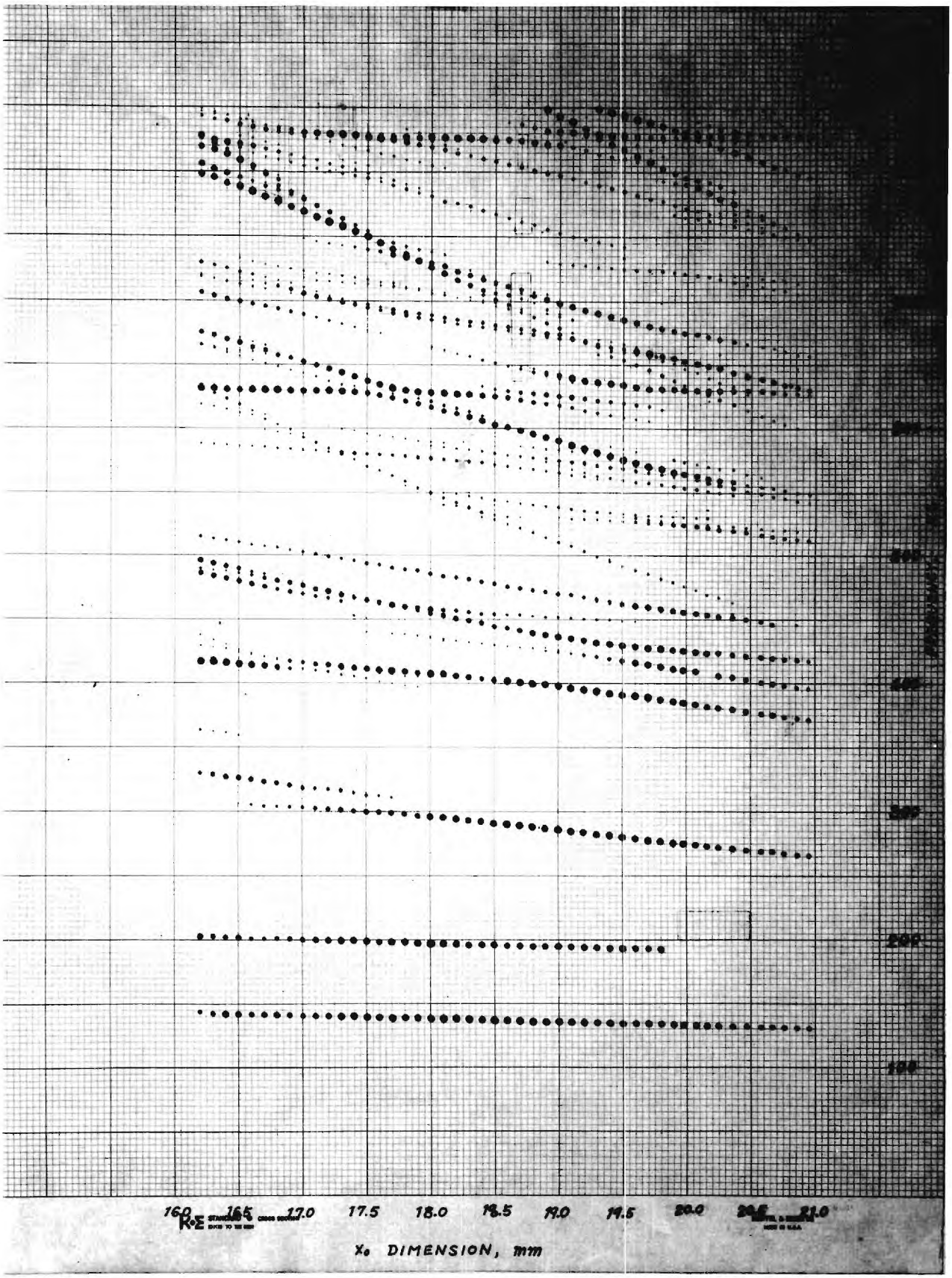

NSF-G18972 Fig. 1 Low Frequency Responses

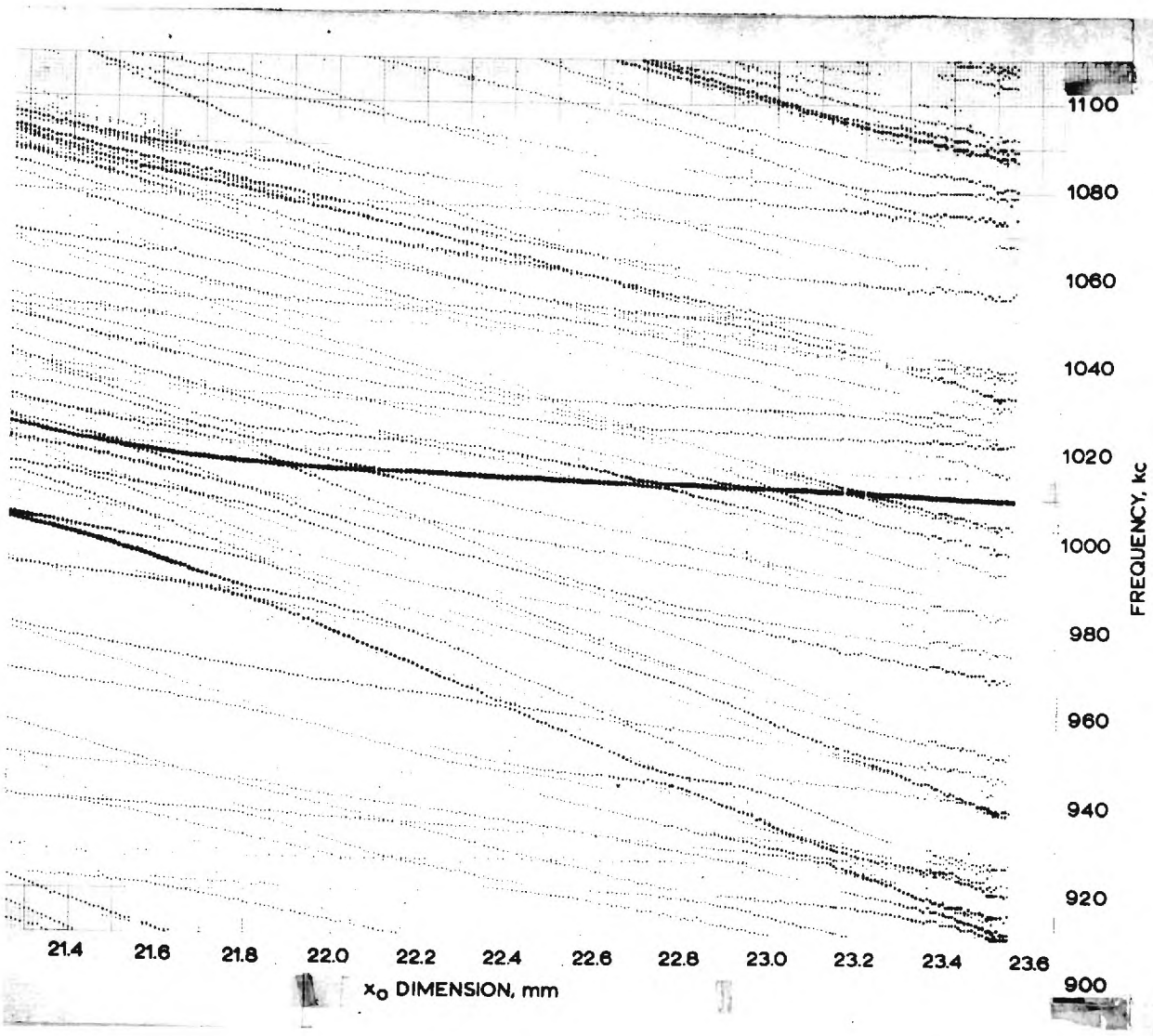

NSF-G18972

Fig. 2

Fundamental (a)

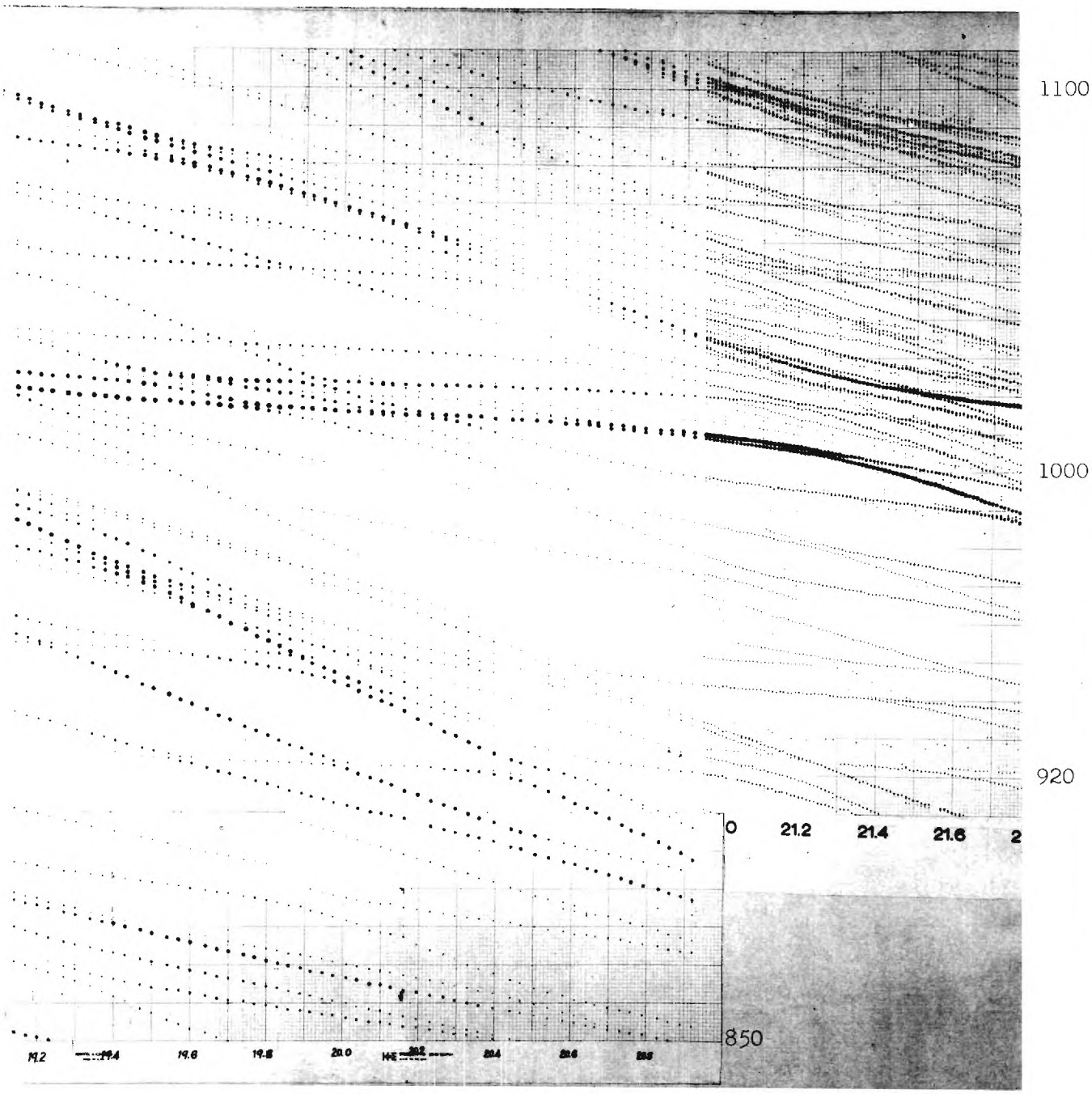

NSF-G18972

Fig. 3

Fundamental (b)

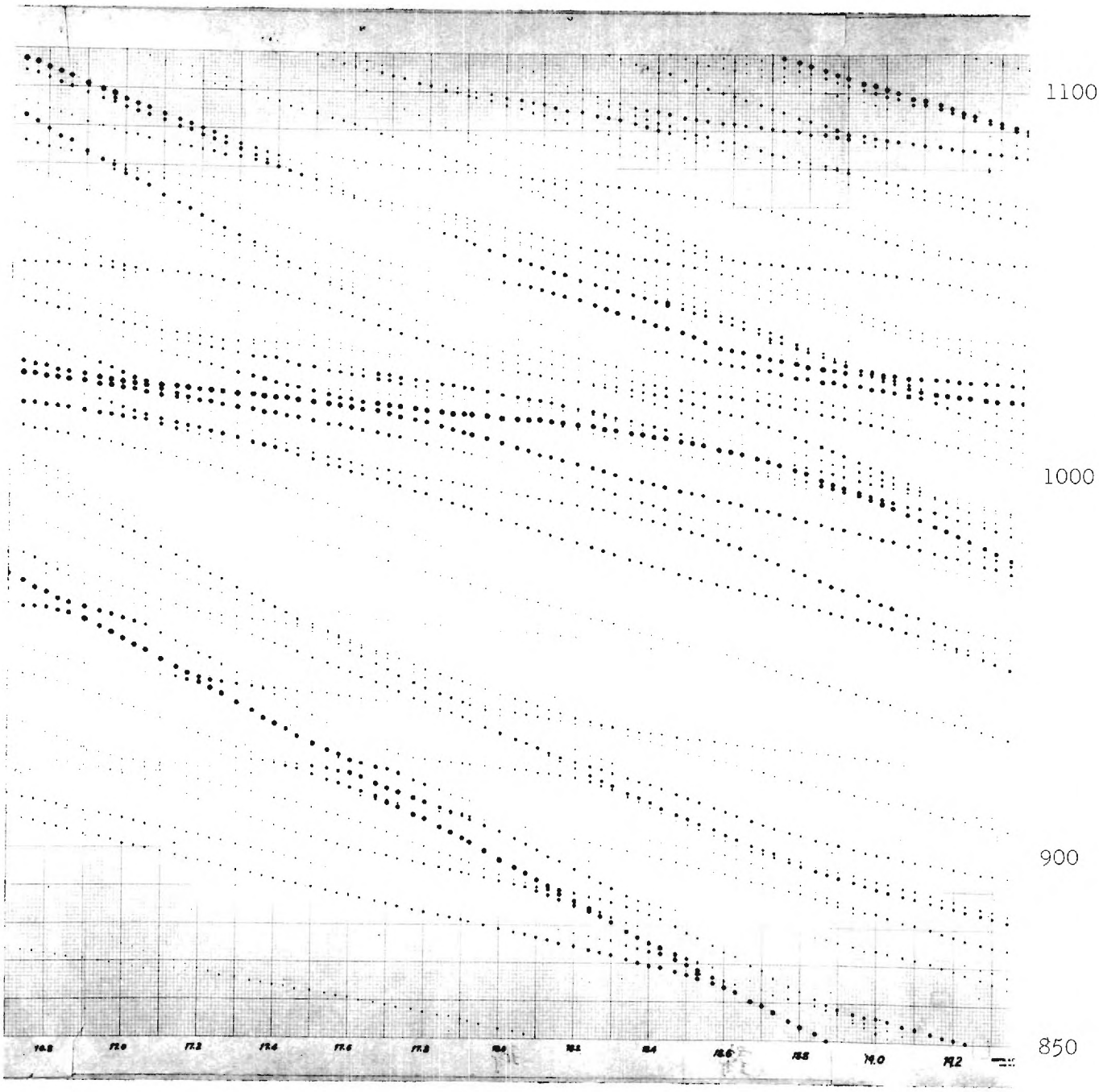

NSF-G18972 Fig. 4 Fundamental (c)

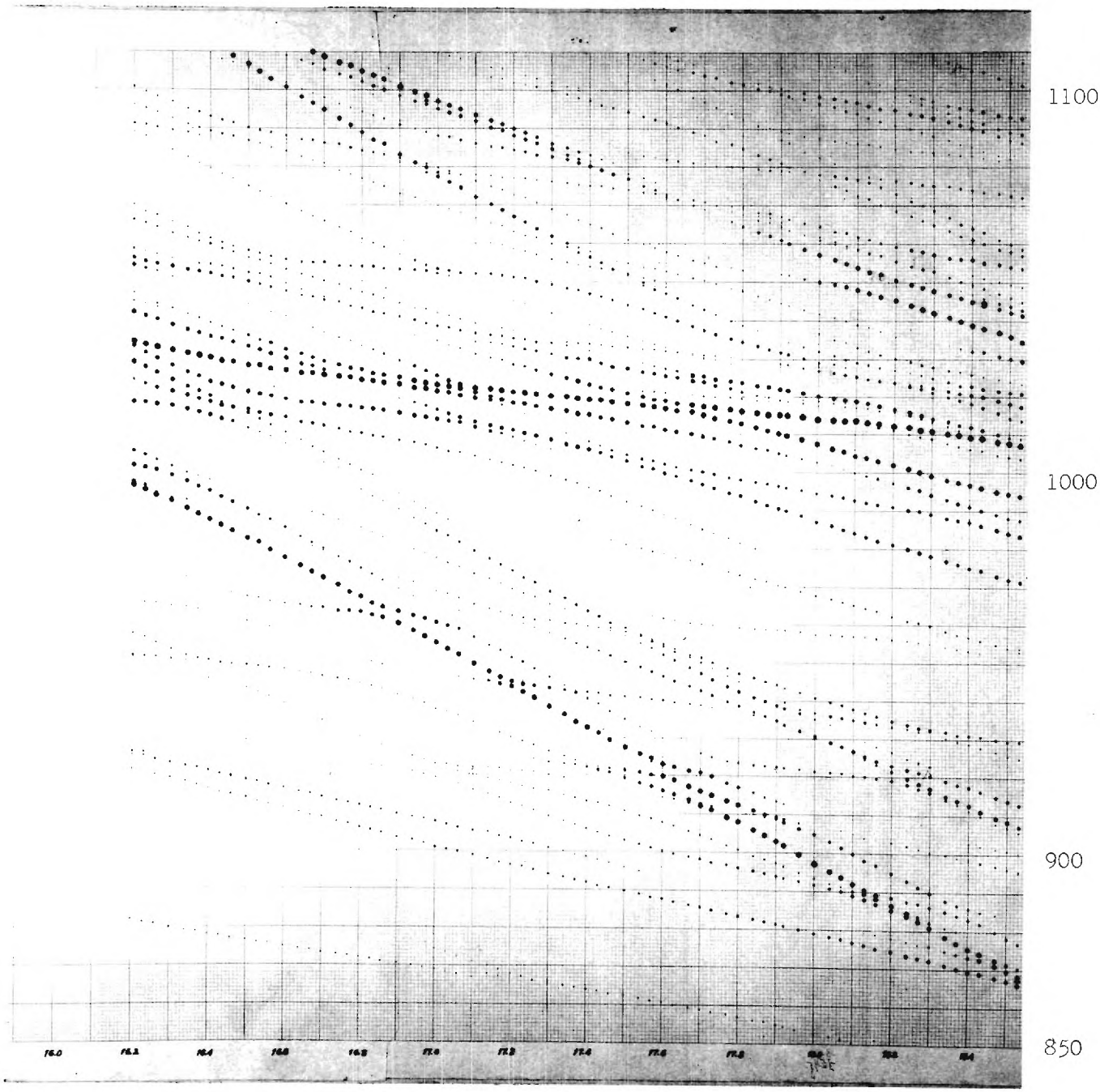

NSF-G18972

Fig. 5

Fundamental (d)

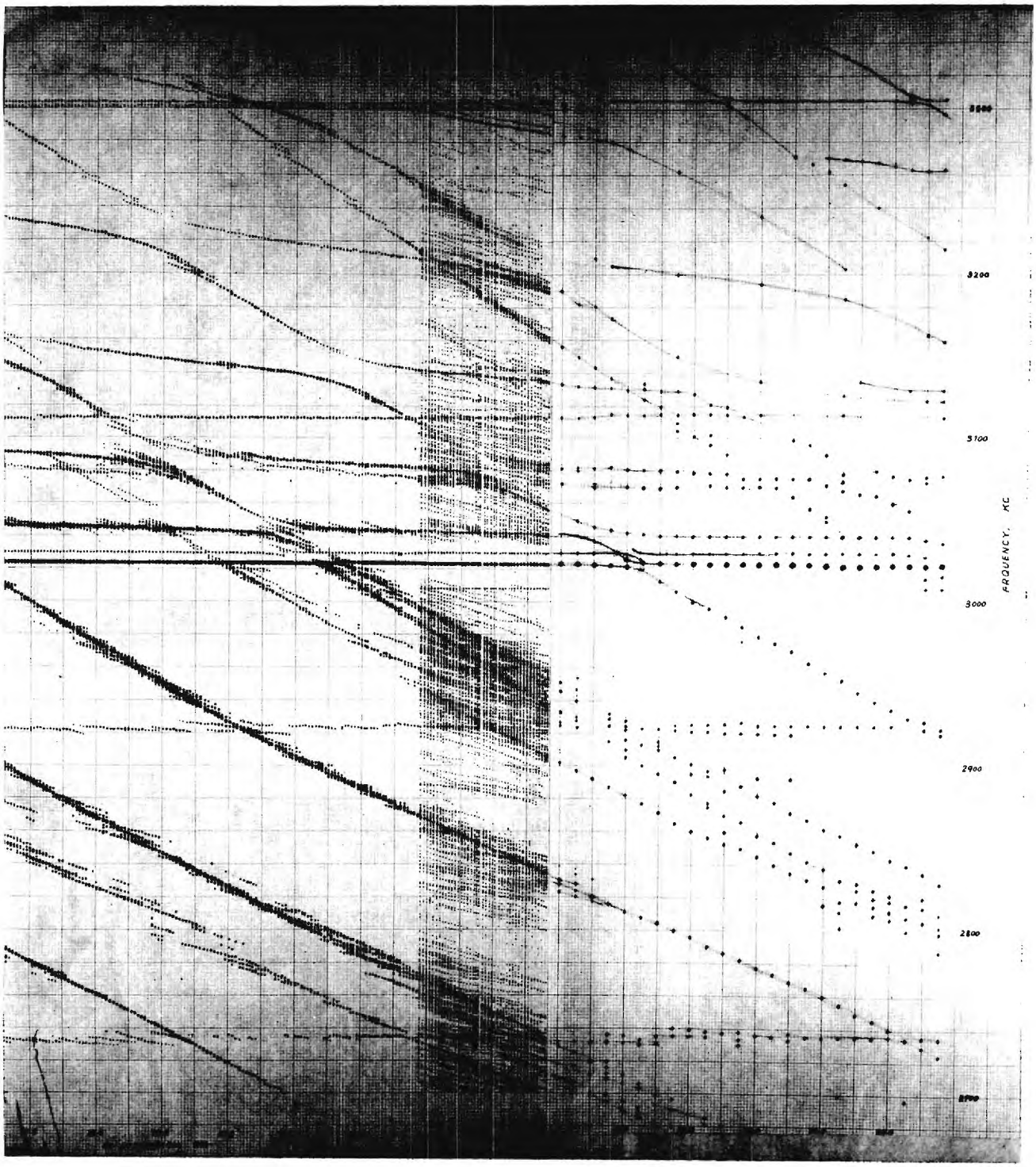

NSF-G18972 Fig. 6 Third Overtone (a)

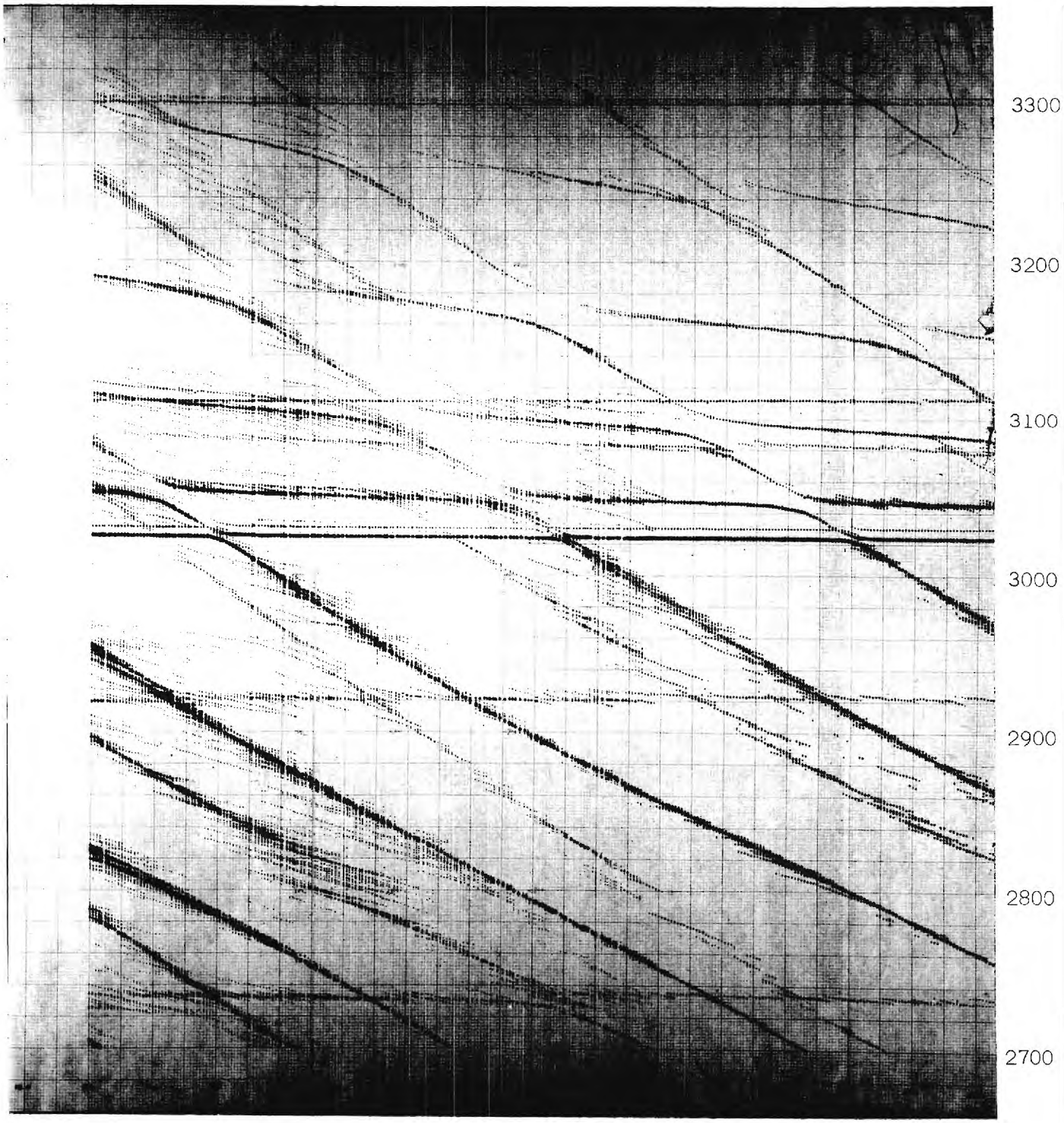

NSF-G18972

Fig. 7

Third Overtone (b)

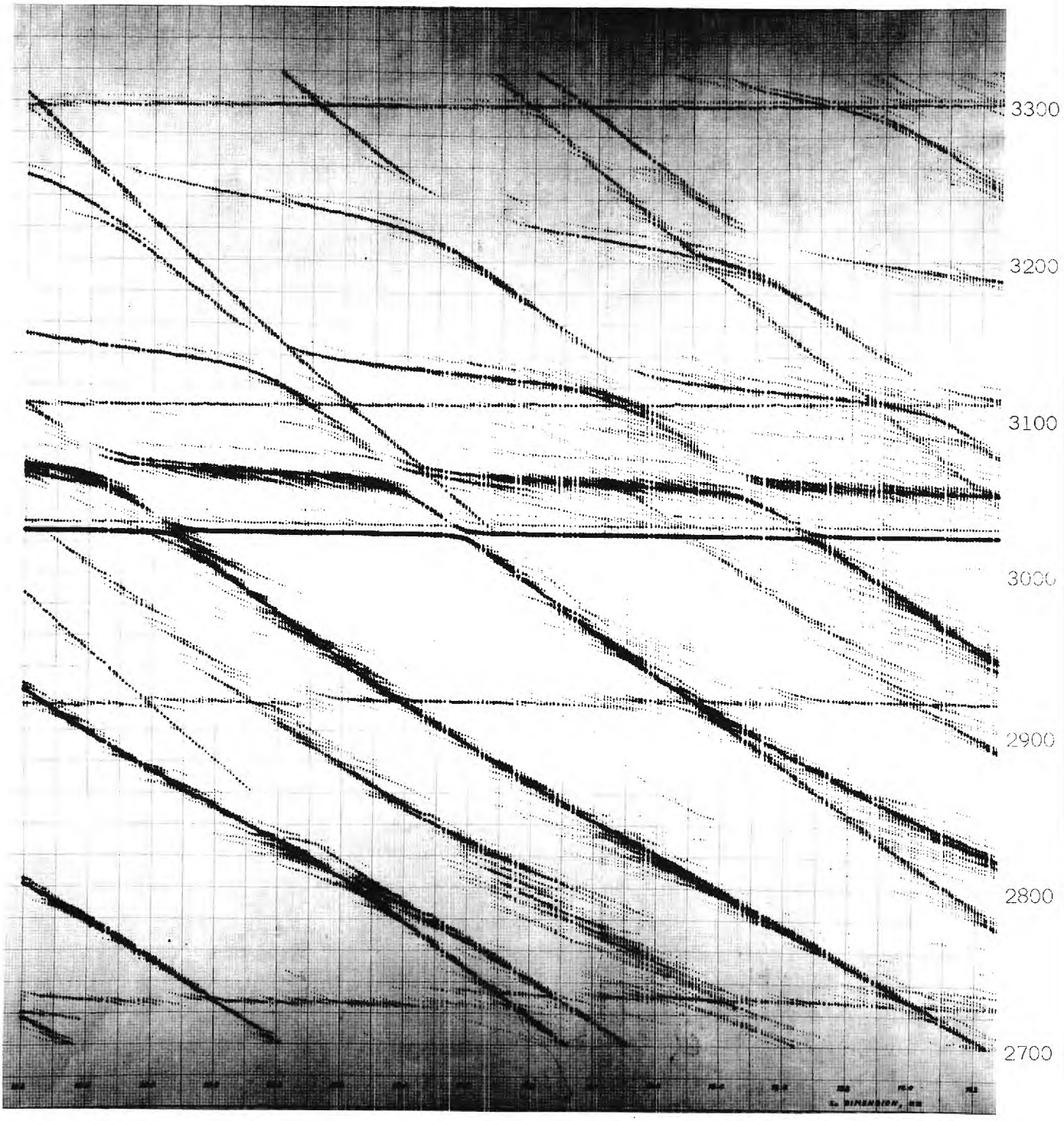

NSF-G18972 Fig. 8 Third Overtone (c)

ENGINEERING EXPERIMENT STATION
GEORGIA INSTITUTE OF TECHNOLOGY
ATLANTA, GEORGIA

FINAL REPORT
PROJECT NO. B-214

MODES OF VIBRATION OF PIEZOELECTRIC QUARTZ CRYSTALS

By

Arthur L. Bennett

NATIONAL SCIENCE FOUNDATION
WASHINGTON, D.C.
RESEARCH GRANT NSF-G18972

1 JULY 1961 TO 30 SEPTEMBER 1963

FINAL REPORT

PROJECT NO. B-214

RESEARCH GRANT NSF-G18972

MODES OF VIBRATION OF PIEZOELECTRIC QUARTZ CRYSTALS

By Arthur L. Bennett

Engineering Experiment Station
Georgia Institute of Technology
Atlanta, Georgia

The purpose of this research is the measurement, analysis, and prediction of the modes of vibration of quartz piezoelectric crystals.

Background

The program for the two-year period covered by this NSF grant is a continuation of the work started in 1958 under the sponsorship of the U.S. Army Signal Research and Development Laboratories. Support was provided during 1960-61 under Grant NSF-G13647.

A series of theoretical papers by Mindlin and associates are available on the prediction of the frequencies of vibration of the various modes which can be excited by a radio frequency voltage applied to surface electrodes on the crystal. That work, as well as the early approximations by Koga, was based on the differential equations governing the motion of the crystal. The latest paper by Mindlin[1*] provides an excellent representation of the measurements by Fukuyo[2]. The theory does not include, however, the effect of

*Superscript numbers refer to references listed in Bibliography.

piezoelectric stiffness, and arbitrary constants are introduced to compensate in part for the omission of higher-order terms dependent on the thickness. The elastic constants used in the computation were derived from the experimental data to be fitted. These constants differ as much as one per cent from those reported by Koga[3].

Research Progress

Theoretical. The paper by Koga[4], was completed with substantial participation by the Georgia Tech group. This theory applies to a plate of limited size and in addition elastopiezoelectric stiffness coefficients are introduced to include the piezoelectric effect. Although this contribution to the stiffness has an effect on the computed frequencies of less than one per cent, its inclusion in the theory is desirable.

The procedure in the development of the theory is given in some detail in Interim Technical Report No. 1[5]. This report is a most useful compilation of notation and of the constants of quartz, both in the orthogonal axes and in the rotation corresponding to the AT-cut.

A critical examination of the mathematical procedures employed by Koga has led to some doubt as to the validity of the results. Until this suspicion can be validated or removed, we are reluctant to base further interpretation on the computed results. This uncertainty is most distressing because the theory provided a basis both for comparison with the polarization distribution as noted by Koga[4] and with the strain gradient measured with the x-ray diffraction topography technique.

The theoretical development by Tiersten and Mindlin[6], including the piezoelectric relations and the electric field equations, is being programmed for the calculation of resonance eigen values for comparison with the numerical results of the computation by Mindlin and Gazis[1] and with the experimental data. Our computations are based on the crystal constants of Bechmann[7] whereas Mindlin and Gazis derived constants from experimental data[2] of lower reliability than that acquired under this project.

The feasibility is being examined of extending the theory of Tiersten and Mindlin[6] to include the displacements of higher order than $U_j^{(0)}$, $U_j^{(1)}$, and $U_j^{(2)}$ neglected by the authors. This extension is needed to obtain the strain gradient in the y' direction for comparison with the x-ray measurements.

Experimental. During the first year the resonant frequencies over the range 100 Kc to 1100 Kc and 2700 Kc to 3300 Kc were measured to an x-dimension of 16.2 mm, completing the series from the initial value of 25.56 mm. Plots of the responses are given in the Annual Report for 1961-62. Polarization records of strong responses were made at intervals of about 0.5 mm. A more complete record of responses for a similar crystal 25.56 mm in x was taken.

A group of 10 polished crystals about 25 mm square, fundamental frequency just over 1 Mc, was purchased. The orientation was checked by x-ray and the edges carefully finished to close tolerance. Measurements of these crystals have confirmed the repeatability of the detailed measurements with the first crystal.

Extensive measurements by the Lang[8] technique have served to develop and perfect our application of the technique to the measurement of crystals in vibration. Initial results were published[9].

The effect of crystal drive level on the "rocking curve", that is the apparent angular width of the source, has been investigated. It is found that there is a pronounced widening of the skirts of the curve; also the width of the response at half-height is doubled at a drive level of 6 mA/cm^2 for the fundamental near 1 Mc. Data from the rocking curve is essential for interpretation of intensity measurements of the diffracted beam as the amplitude of oscillation is increased by increase of the driving current. Measurements completed indicate an inflection at about 2 mA/cm^2 for the crystal noted above; the rate of increase diminishes at higher drive levels as predicted.

The physical interpretation of the interaction of the thickness-shear strain with the corresponding shear of the flexure wave propagated in the x-direction is more consistent with both the observed polarization and diffraction patterns than alternate hypotheses.

The spectrum recording equipment has been improved by the addition of new equipment. A stable signal generator is used to drive the crystal in a 50-ohm series impedance circuit. The voltage across the output is recorded on a logarithmic scale through the use of a commercial log amplifier and an oscillograph with 3 Kc response. A special transformer was constructed to balance out the constant capacity of the crystal and permit a direct measurement of the motional resistance.

The polarization measurement equipment has been improved to record phase information thereby removing the possible ambiguity in interpretation. The table and translation mechanism have been redesigned to take the larger crystals to be used in the continuation of the work.

In general, the second year has reflected the transition from the survey of the detailed behavior of a single crystal to the development of better equipment for the wider field of investigation planned for the future. The full evaluation of the measuring techniques and elimination of spurious effects, more troublesome than at first anticipated, has been of great value in the interpretation of the results.

Personnel

Dr. Koga spent July and part of August 1961 at Georgia Tech. Mr. Masahiro Toki, graduate student at Yokohama National University, started work on July 1, 1961. Mr. Toki continued the measurements of crystal D-1 with diligence and efficiency until July 1962 when he went to the University of Minnesota for graduate work.

Dr. G. C. Knollman left Georgia Tech for industrial employment. During the fall of 1962, Dr. Dar Veig Ho, Assistant Professor of Mathematics, started part-time analytical work and theoretical investigations. He was joined full-time during the summer by Mr. W. F. Martens, second year graduate student in Math.

During the spring of 1962, Mr. Norval K. Hearn, Jr., Assistant Research Physicist under the guidance of Dr. Young, Research Associate Professor of Physics, assisted substantially in developing the Lang technique of x-ray diffraction topography. He assisted occasionally until the fall of 1963 when he entered the graduate school of Kansas State University. During the spring of 1963, Mr. K. R. Allen, graduate student in Physics assisted with the x-ray work.

Mr. J. I. Cochran, graduate student in Electrical Engineering worked part-time from April 1962 to December when he left for industrial employment. He was succeeded by Mr. H. G. Henderson, graduate student in Electrical Engineering, who has continued the work on the electronics equipment.

Mr. M. T. Spahr, Physics graduate student, completed his undergraduate work in March 1963 at which time he joined the project. He has participated in the analysis of data and in programming for the B-220 and B-5000 computers.

BIBLIOGRAPHY

1. R. B. Mindlin and D. C. Gazis, "Strong Resonances of Rectangular AT-cut Quartz Plates." Contracts Nonr-266(09) and Signal Corps Contracts DA36-039 SC-87414, July 1961.

2. I. Koga and H. Fukuyo, J. Inst. Elec. Comm. Engrs. of Japan, 36, 59, (1953), also Hitohiro Fukuyo, Bulletin of the Tokyo Institute of Technology, Series A, 1955, No. 1.

3. I. Koga, et al., Phys. Rev. 109, 1467 (1958).

4. Issac Koga, "Radio-Frequency Vibrations of Rectangular AT-cut Plates," J. Appl. Phys., 34, 2357-65 (1963).

5. Gilbert C. Knollman, "Coupled Thickness-shear and Flexure Vibrations in Rectangular AT-cut Quartz Plates," Interim Technical Report No. 1, Project B-214.

6. H. F. Tiersten and R. D. Mindlin, "Forced Vibrations of Piezoelectric Crystal Plates," Quart. Appl. Math., 20, 107-119, (1962).

7. R. Bechmann, "Elastic and Piezoelectric Constants of Alpha-Quartz," Phys. Rev., 110, 1060-1 (1958).

8. A. R. Lang, "Studies of Individual Dislocations in Crystals by X-Ray Diffraction Microradiography." J. Appl. Phys. 30, 1748 (Nov. 1959).

9. Arthur L. Bennett, R. A. Young, and Norval K. Hearn, Jr., "X-Ray Diffraction Topography of Vibrating Quartz Crystals," Appl. Phys. Letters, 2, 154-6 (1963).